Seasonality of the Quasi-biennial Oscillation signal in water vapor in the tropical stratosphere

Qian Lu[1, 3], Jian Rao[1, *], Chunhua Shi[1], and Chaim I. Garfinkel[2]

[1]Collaborative Innovation Center on Forecast and Evaluation of Meteorological Disasters / Key Laboratory of Meteorological Disaster of Ministry of Education, Nanjing University of Information Science and Technology, Nanjing 210044, China
[2]Fredy and Nadine Herrmann Institute of Earth Sciences, The Hebrew University of Jerusalem, Givat Ram, Jerusalem, Israel
[3]Department of Basic Education, Tangshan University, Tangshan 063000, China

Correspondence to: Dr. Jian Rao (raojian@nuist.edu.cn)

Abstract. The feedback of water vapor has an impact on global temperature changes, and stratospheric water vapor ~~more specifically~~ can directly affect~~s~~ the radiative balance and temperature structure of the stratosphere.~~Stratospheric water vapor is an important greenhouse gas, which affects the radiation balance and temperature structure of the stratosphere and troposphere.~~ Although previous studies have investigated the water vapor variability associated with the quasi-biennial oscillation (QBO), the seasonal difference~~s~~ in the water vapor QBO are still not well understood. Using the ERA5 reanalysis and SWOOSH observations, this study compares the stratospheric water vapor distribution in northern winter and summer under different QBO phases. The 30 hPa QBO index exerts the greatest influence on 100 hPa water vapor at a lag of six months.~~The water vapor and zonal winds are positively correlated in the mid-to-lower stratosphere~~ During northern summer, the peak amplitude of 100 hPa water vapor under different QBO phases in tropical regions reaches ±0.12 ppm at a six-month lag, while in winter it reaches ±0.2 ppm. The dehydration effect by cold temperature in the lower stratosphere is also more effective in boreal winter than in summer.~~; however this relationship weakens in the northern summer.~~ The intensity of the QBO-related ~~residual~~ secondary circulation is stronger in the boreal winter than in summer, which not only influences the cold point tropopause temperature in tropical regions but also drives the transport of stratospheric water vapor. The mean vertical transport term via the ~~QBO related~~QBO-related residual circulation is the leading factor controlling the water vapor distribution in the tropical lower~~most of the~~ stratosphere.~~ This dynamic transport of water vapor in the lower stratosphere by the residual circulation is larger in boreal winter than in summer. Further, the dehydration effect by cold temperature in the lower stratosphere is also more effective in boreal winter than in summer. Tropical deep convection exhibits opposite variations for a given QBO phase in boreal winter versus summer especially over the Indo-Pacific Oceans. This further enhances the temperature difference between the QBO easterly and westerly phases in winter and reduces the temperature contrast in summer.~~ Although the CMIP6 models simulated the lagged effect of the 30 hPa QBO on lower stratospheric water vapor,~~It is still a challenge for models to reproduce the water vapor QBO:~~ ~~CMIP6 models~~they tend to underestimate the water vapor ~~QBO~~ amplitude, and the seasonal contrast ~~in the water vapor QBO between boreal winter and summer~~ is underrepresented in most models.

1 Introduction

The feedback of water vapor (WV) has an impact on global temperature changes~~Water vapor is the dominant greenhouse gas in the atmosphere~~ (Held and Soden, 2000~~Held, 2000~~; Dessler et al., 2013; Solomon et al., 2010), and stratospheric water vapor (SWV) more specifically affects the radiative balance and temperature structure of the stratosphere (Bi et al. 2011; Xia et al. 2021). It can also further affect the stratospheric circulation through the mutual adjustment relationship between thermodynamic balance and dynamic balance (Banerjee et al., 2019; Charlesworth et al., 2023; de Forster and Shine, 1999). In addition, it also modulates chemical processes in the stratosphere,~~,~~ and ~~such as~~ the increase in SWV, for example, has a slight impact on ozone depletion~~ozone depletion~~ (Tian et al., 2009, 2023; Wohltmann et al., 2024).

W~~ater vapor~~V can enter the stratosphere through different channels (Lu et al., 2020; Mote et al., 1996; Randel et al., 2015; Randel and Park, 2019; Tinney and Homeyer, 2023; Yue et al., 2019). The WV in the stratosphere mainly comes from the upward transport of tropospheric WV in the tropics~~The primary channel through which tropospheric water vapor enters the stratosphere is the tropical path~~ (Evan et al., 2015; Garfinkel et al., 2013; Mote et al., 2000; Randel and Park, 2019), where cold temperatures at the tropopause determine the tropospheric ~~water vapor~~WV content entering the stratosphere (Hardiman et al., 2015; Xia et al., 2019). These cold temperatures freeze and condense most of the ~~water vapor~~WV that approaches the tropopause. As a consequence, most of the ~~water~~ WV that enters the tropopause transition layer falls back to the troposphere, and only a tiny part of the ~~water vapor~~WV eventually reaches the stratosphere (Brewer, 1949; Dessler et al., 2013; Holton and Gettelman, 2001; Ueyama et al., 2016; Xia et al., 2019).

As a leading mode of interannual variability in the equatorial stratosphere, the quasi-biennial oscillation (QBO) completes a cycle every 28 months on average (Baldwin et al., 2001; Rao et al., 2020a). During a QBO cycle, alternating easterly and westerly winds propagate downwards from the equatorial upper stratosphere to the tropopause (Baldwin et al., 2001; Cai et al., 2022; Rao et al., 2020b, 2023a, b). The QBO is primarily driven by wave fluctuations of different scales in the tropics. Waves propagating upward carry zonal momentum, and the momentum of westerly or easterly winds is deposited into the stratosphere after wave breaking (Coy et al., 2017; Lindzen and Holton, 1968; Wang et al., 2023). It is observed that the intensity of the QBO easterly phase (30–35 m s^{-1}) is usually stronger than that of westerly phase (15–20 m s^{-1}), with the QBO amplitude maximized around 20–30 hPa (Anstey et al., 2022; Baldwin et al., 2001). The maintenance and transition of the QBO westerly and easterly phases are related to tropical wave activities, including Kelvin waves, mixed Rossby–gravity waves, and internal gravity waves (Canziani and Holton, 1998; Randel and Wu, 2005; Richter et al., 2014a; Holt et al., 2016; Kang et al., 2020; Bramberger et al., 2022; Garfinkel et al., 2022; Pahlavan et al., 2023). However, it remains a challenge to simulate the QBO in general circulation models (GCMs), with only a few GCMs being able to reproduce it. The waves need to be correctly represented to simulate a realistic QBO. ~~But m~~Many GCMs still cannot simulate a realistic spectrum of tropical waves because of their low resolution and their deficiencies in the parameterization of small-scale gravity waves forcing (Ricciardulli and Garcia, 2000; Lott et al., 2014). Studies have suggested that an adequately fine vertical resolution (vertical grid spacing of ~500–700 m) of the troposphere and lower stratosphere is also necessary to simulate the QBO due to the forcing

of some resolved waves with small vertical wavelength and the need to capture the wind shear (~~Giorgetta et al., 2006;~~ Richter et al., 2014~~b~~; Geller et al., 2016). In CMIP5, only five models could generate the QBO internally (~~(Schenzinger et al., 2017;~~ Butchart et al., 2018). In CMIP6, at least 15 models now able to simulate realistic QBO-like behavior during the historical period (Richter et al., 2020~~Richter, Anstey, et al., 2020~~).

The evolution of the tropical stratospheric QBO is accompanied by the downward propagation of temperature anomalies (Baldwin et al., 2001; Rao et al., 2020a), which directly affects the freezing temperature of ~~water vapor~~WV entering the stratosphere (Hardiman et al., 2015; Tao et al., 2015). The QBO winds are in balance with an anomalous secondary circulation, which both modulates the BD circulation and affects the distribution of chemical components (e.g., ozone, methane, water vapor) in the stratosphere (Baldwin et al. 2001). This anomalous secondary circulation can also explain the stratospheric temperature anomalies associated with adiabatic motions (Baldwin et al., 2001; Lu et al., 2020; Rao et al., 2019), which in turn affect ~~water vapor~~WV entering the stratosphere (Tian et al., 2023; Xia et al., 2021; Ziskin ~~Ziv~~ et al., 2022). Previous work has evaluated the QBO ~~water vapor~~WV effect in a subset of CMIP6 models, and found they qualitatively capture but underestimate the QBO effect (Ziskin et al. 2022). The QBO leads to a change of static stability in the tropical lower stratosphere and tropopause, further adjusts deep convection activities, and affects the upward transport of tropical ~~water vapor~~WV (Dong et al., 2020; Tselioudis et al., 2010).

The relationship between the QBO and tropical stratospheric ~~water vapor~~WV has been widely investigated (Chen et al., 2005; Tao et al., 2015; Xia et al., 2021). However, it still remains unclear whether the effects of the QBO on ~~stratospheric water vapor~~SWV differ between northern winter and summer. The seasonality of the ~~water vapor~~SWV QBO signal has been seldom studied. Serva et al. (2022) found that there are seasonal differences in temperature and SWV in tropical regions. In the northern summer, the temperature at 100 hPa and the WV at 85 hPa reach their peaks, while in winter, they reach their lowest levels (Serva et al., 2022). The QBO is affected by the BD circulation, and it is stronger in northern winter than in summer (Butchart, 2014). Tegtmeier et al. (2020) found that the temperature amplitude of QBO was 2 K in February of northern winter and only 0.9 K in September of summer ~~(Tegtmeier et al., 2020)~~. ~~Then~~Similar questions naturally arise:~~,~~ D~~d~~oes the amplitude of WV QBO also undergo a similar change? What are the differences between winter and summer? The research on the seasonal differences of WV QBO not only deepens the multi-time scale understanding of the stratospheric and tropospheric coupling, but also provides a scientific basis for cross-seasonal climate prediction ~~and the formulation of ozone layer protection policies, such as considering seasonally dependent emission control policies~~. This study uses more samples based on the long time series of the QBO signal in SWV~~stratospheric water vapor~~ and discusses the differences in ~~stratospheric water vapor~~SWV distribution between different QBO phases and between different seasons. Possible causes of those differences are diagnosed, and the performance of climate models in capturing the QBO signal in ~~water vapor~~WV is also evaluated (Ye et al., 2018; Ziskin ~~Ziv~~ et al., 2022).

The organization of this article is as follows. In section 2, a brief description of datasets and methods is given. Section 3 presents the timeseries of the ~~water vapor~~WV QBO. Section 4 compares differences in the distribution of ~~stratospheric water vapor~~SWV anomalies associated with the QBO between boreal winter and summer. Possible mechanisms responsible for the

seasonal difference in the ~~stratospheric water vapor~~SWV signal are also discussed. Section 5 evaluates the simulation of the ~~stratospheric water vapor~~SWV QBO by CMIP6 models. Finally, conclusions are provided in section 6.

2 Data and methods

a. Datasets

To investigate the ~~stratospheric water vapor~~SWV QBO in the tropical stratosphere, the European Centre for Medium-Range Weather Forecasts' fifth generation reanalysis (ERA5) from 1960 to 2020 (Hersbach et al., 2020) was used. The horizontal resolution of the ERA5 reanalysis is 0.25° (latitude) × 0.25° (longitude), and the model has 137 levels in the vertical direction from 1000 to 0.01 hPa. A horizontal resolution of 1° (latitude) × 1° (longitude) at 37 pressure levels from 1000 to 1 hPa in the vertical direction was collected for this study. The variables used include zonal and meridional wind, specific humidity, and air temperature on pressure levels.

The Stratospheric Water and Ozone Satellite Homogenized (SWOOSH) dataset version 2.7 is also used in this paper. It is a merged record of stratospheric ozone and ~~water vapor~~WV measurements taken by a number of limb sounding and solar occultation satellites over the previous ~40 years (1984 to present). This dataset is a combination of different data sources, including SAGE-II/III/ISS, UARS HALOE, UARS MLS, Aura MLS, ACE-FTS, and OMPS-LP (Davis et al., 2016). The SWOOSH data ~~mainly consists of~~provide monthly averages, standard deviation, number of observations and average uncertainty on the pressure grid~~. The grid-based data includes the average value, standard deviation, number of observations and average uncertainty~~ measured by each satellite instrument. SWOOSH~~It~~ also includes combined (multi-instrument) products based on the weighted average of available measurement values. A key aspect of the merged product is that the source records are homogenized to account for inter-satellite biases and to minimize artificial jumps in the record, producing a long-term data record~~ that is both homogeneous (i.e., with minimal artificial jumps in time) and accurate (i.e., unbiased)~~. Since the UARS HALOE observation data began on 19 October 1991, we have used SWOOSH data from 1992 onwards.

In contrast to the troposphere, the ~~water vapor~~WV content within the stratosphere is extremely low. Compared to the SWOOSH satellite observation data, the ERA5 reanalysis data provides a longer time ~~scale~~span, which ~~provided~~provides more samples for revealing the effect of QBO on ~~stratospheric water vapor~~SWV. There remains uncertainty regarding the performance of ERA5 reanalysis data in depicting ~~stratospheric water vapor~~SWV. In the ERA5 reanalysis, ~~water vapor~~WV mainly assimilates in-situ humidity observations in the troposphere and satellite radiation observations that are only sensitive to humidity in the troposphere. Therefore, the ~~stratospheric water vapor~~SWV in ERA5 reanalysis data is a GCCM output with specified dynamics (Hersbach et al., 2020). From 2000 to 2006, ERA5 showed cold deviation in the lower stratosphere. The global average temperature of the stratosphere and tropospheric apex corrected by ERA5.1 was better than that of ERA5 (Simmons et al., 2020). Previous studies have shown a wet bias in the tropical tropopause in the ERA5 reanalysis data (Krüger et al., 2022). Some studies also found that the content of ~~stratospheric water vapor~~SWV in ERA5 was superior to that of ERA-Interim (Wang et al., 2020). We use SWOOSH satellite monitoring data to validate the applicability and uncertainty of ERA5

reanalysis data in ~~stratospheric water vapor~~SWV. Figure 1 shows the evolution of the annual mean, summer mean, and winter mean of the ~~water vapor~~WV mixing ratio in the troposphere during SWOOSH satellite data and ERA5 reanalysis from 1992 to 2019. Compared to SWOOSH satellite data, ERA5 can better display the distribution pattern of ~~stratospheric water vapor~~SWV, and the ~~water vapor~~WV content is basically consistent. The ~~water vapor~~WV content in ERA5 has a 0.3 ppm moisture deviation at the bottom of the tropical stratosphere, which is reflected in the annual mean, summer mean and winter mean, consistent with previous analyses (Krüger et al., 2022). However, at the top of the stratosphere, the ~~water vapor~~WV content ~~shown by~~in ERA5 ~~in tropical and polar regions~~ is all relatively low.

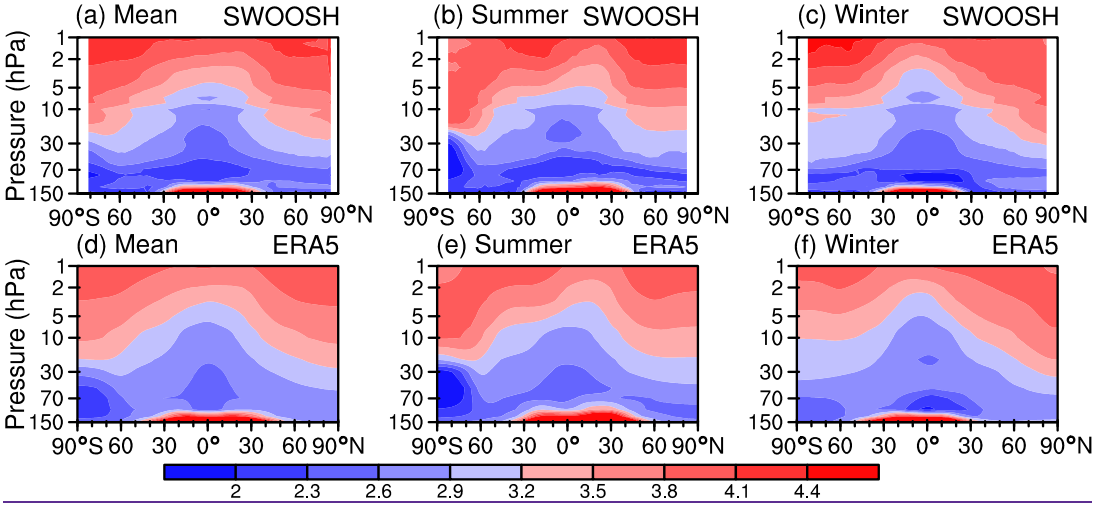

Figure 1. Comparative analysis of ~~stratospheric water vapor~~SWV from SWOOSH satellite observations and ERA5 reanalysis during 1992–2019 (unit: ppm). Panels a-c in the first row ~~shows~~show ~~stratospheric water vapor~~SWV from SWOOSH observations, while panels d-f in the second row display ~~stratospheric water vapor~~SWV derived from ERA5 reanalysis. (a, d) Multi-year mean ~~stratospheric water vapor~~SWV mass mixing ratio. (b, e) Mean ~~stratospheric water vapor~~SWV mass mixing ratio in northern summer. (c, f) Mean ~~stratospheric water vapor~~SWV mass mixing ratio in northern winter.

To understand the possible climatic effects of ~~stratospheric water vapor~~SWV and its representation in models, this study also evaluates the historical simulations of ~~water vapor~~WV QBO from 18 models with internally generating QBO from Phase 6 of the Coupled Model Intercomparison Project (CMIP6) (Eyring et al., 2016; Simpkins, 2017). They are ACCESS-CM2, AWI-CM-1-1-MR, BCC-CSM2-MR, CESM2-WACCM-FV2, CESM2-WACCM, CNRM-CM6-1, E3SM-1-0, E3SM-1-1, EC-Earth3-VEG, EC-Earth3, GFDL-ESM4, HadGEM3-GC31-LL, HadGEM3-GC31-MM, IPSL-CM6A-LR, MIROC6, MPI-ESM1-2-HR, MRI-ESM2.0, and UKESM1-0-LL. The historical simulation is a mandatory historical climate experiment from 1850 through 2014 under all observation-based and time-varying forcings (i.e., greenhouse gas concentrations, aerosols, ozone depletion, solar cycles, and land use) (Eyring et al. 2016). We only used the first historical run of the CMIP6 models, and all models provide specific humidity. Previously, some studies found that the CMIP6 models underestimate the ~~water vapor~~WV content at the bottom of the tropical stratosphere (Keeble et al., 2021; Ziskin et al., 2022).

b. Methodology

The climatology of a variable is calculated as long-term monthly average over the time period from 1960 to 2020. The anomaly refers to the deviation of the monthly data from the monthly climatology with the trend removed for each calendar month. A Butterworth first-order bandpass filter was used to extract the ~~water vapor~~WV variations at the period of 15-60 months, mimicking the ~~water vapor~~WV QBO (Krishnamurti et al., 1990; Murakami, 1979).

The QBO index is defined as the stratospheric zonal mean zonal wind anomalies over the equator at 5°S - 5°N (Baldwin et al. 2001; Rao et al. 2020a). Considering that the QBO wind variability is maximized around 30 hPa and for many CMIP models the QBO signal is not present below 30 hPa, the QBO index at 30 hPa is employed. QBO events are selected when the QBO index is greater than 5 (less than -5) m/s to build the westerly QBO (easterly QBO) composites, following previous studies (e.g., Rao et al. 2020a, 2020b).

To accurately diagnose the driving factors of the zonal mean distribution of ~~stratospheric water vapor~~SWV under different QBO conditions, we use the transformed Eulerian-Mean (TEM) tracer continuity equation under spherical z coordinates as follows (Garcia and Solomon, 1983; Monier and Weare, 2011):

$$\frac{\partial \bar{\chi}}{\partial t} = -\frac{\bar{v}^*}{a}\frac{\partial \bar{\chi}}{\partial \phi} - \bar{w}^*\frac{\partial \bar{\chi}}{\partial z} - \frac{1}{\rho_0}\nabla \cdot \mathbf{M} + \bar{S}, \quad (1)$$

where χ is the mixing ratio of ~~water vapor~~WV, $\bar{v}^*$ and $\bar{w}^*$ are the horizontal and vertical velocities of the transformed Eulerian mean residual circulation. The residual velocities are calculated as follows (Butchart, 2014; Hardiman et al., 2014):

$$\bar{v}^* = \bar{v} - \frac{1}{\rho_0}\frac{\partial}{\partial z}\left(\rho_0 \frac{\overline{v'\theta'}}{\bar{\theta}_z}\right), \quad (2)$$

$$\bar{w}^* = \bar{w} + \frac{1}{a\cos\phi}\frac{\partial}{\partial \phi}\left(\cos\phi \frac{\overline{v'\theta'}}{\bar{\theta}_z}\right). \quad (3)$$

In Eqs. 2 and 3, $\bar{v}^*$ represents the residual meridional wind component, $\bar{w}^*$ is the residual vertical wind component, θ denotes potential temperature, a stands for Earth's radius, ϕ signifies latitude, and ρ_0 indicates air density. The overbar denotes zonal averaging, and prime denotes zonal deviations. $\nabla \cdot \mathbf{M}$ is the divergence of the eddy flux vector and represents the eddy transport of ~~water vapor~~WV (In the case of a non-inert tracer, it doesn't represent the full eddy transport, which is partly already included in the residual term). The components of the eddy flux vector M are defined as follows (Garcia and Solomon, 1983):

$$M^{(\phi)} = \rho_0\left(\overline{v'\chi'} - \frac{\overline{v'\theta'}}{\bar{\theta}_z}\frac{\partial \bar{\chi}}{\partial z}\right), \quad (4)$$

$$M^{(z)} = \rho_0\left(\overline{w'\chi'} + \frac{1}{a}\frac{\overline{v'\theta'}}{\bar{\theta}_z}\frac{\partial \bar{\chi}}{\partial \phi}\right). \quad (5)$$

The eddy flux vector represents the mass flux of ~~water vapor~~WV by eddies. Finally, $\bar{S}$ in Eq. 1 is calculated as the residual of the other terms, which includes the terms of chemical net production of ~~water vapor~~WV, evaporation (or condensation), and ~~water vapor~~WV eddy transport generated by small-scale disturbances.

3 Stratospheric water vapor QBO behaviour

In terms of data and methods, we compared ERA5 reanalysis with SWOOSH satellite monitoring data and found that ERA5 reanalysis data could reproduce the distribution pattern of SWV (Fig. 1). ERA5 reanalysis can well display the QBO signal of SWV below 10 hPa ~~(Fig. 2)~~. To observe the QBO characteristics of ~~water vapor~~SWV in the tropics~~al stratosphere~~, the ~~water vapor~~SWV anomalies in the tropics were filtered for the periodicities of 15–60 months using a Butterworth first-order bandpass filter (Murakami 1979; Krishnamurti et al. 1990). Figure ~~1~~2 shows the evolution of ~~water vapor~~SWV anomalies in the tropics~~al stratosphere~~ over the past 60 years for the ERA5 reanalysis and 30 years for the SWOOSH data. In the ERA5 reanalysis, ~~water vapor~~SWV in the lower ~~tropical~~ tropics stratosphere around ~~50~~30–100 hPa presents obvious QBO variations, and the maximum amplitude after bandpass filtering can reach ±0.35 ppm. The maximum ~~water vapor~~SWV anomalies in the lower stratosphere subsequently propagate upward to the middle stratosphere, and reach around 10–30 hPa after a year. The amplitude of the ~~water vapor~~WV QBO also gradually weakens during the upward propagation, and the maximum amplitude of the ~~water vapor~~WV anomalies at 10–30 hPa ~~are~~ is only ±0.15 ppm (Fig. 2a). ~~The water vapor in the upper stratosphere around 1–5 hPa also exhibits obvious QBO variability (Fig. 1a, 1b)~~. The ~~water vapor~~WV QBO from SWOOSH is consistent with ERA5 reanalysis, but the amplitude is stronger. ~~, and t~~The strong ~~amplitude~~WV QBO in SWOOSH propagates upward at a higher level. (Fig. ~~1c~~2b). ~~Since HALOE started from 1992, the water vapor QBO amplitude in the upper stratosphere between 1–5 hPa has increased, which is also shown in ERA5 reanalysis. Alternately, the lack of a water vapor QBO in the upper stratosphere before 1992 in ERA5 could be a reanalysis artifact.~~ By comparison, ~~we~~it is found that although there are some differences in the ~~stratospheric water vapor~~SWV QBO between the SWOOSH satellite data and the ERA5 reanalysis data, the ERA5 reanalysis data reproduce~~d~~ the distribution pattern of ~~water vapor~~WV propagation from the lower stratosphere to the upper stratosphere below 10 hPa. Therefore, the long-term data from ERA5 reanalysis can still be used to diagnose the influence and ~~regulation mechanism of~~ dynamics ~~and thermal effects on~~ of ~~water vapor~~WV in the middle and lower stratosphere below 10 hPa. Our subsequent analysis mainly uses ERA5 reanalysis data.

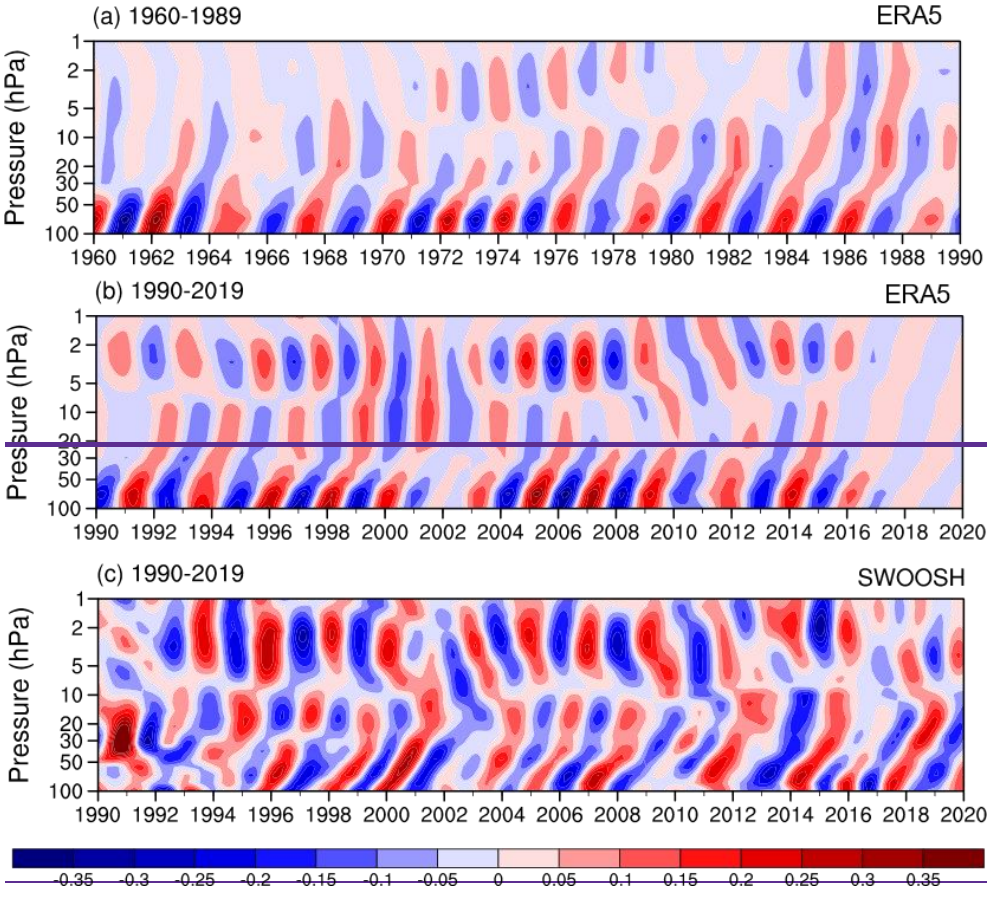
(a) 1960-1989
ERA5
Pressure (hPa)
1
2
5
10
20
30
50
100
1960 1962 1964 1966 1968 1970 1972 1974 1976 1978 1980 1982 1984 1986 1988 1990
(b) 1990-2019
ERA5
Pressure (hPa)
1990 1992 1994 1996 1998 2000 2002 2004 2006 2008 2010 2012 2014 2016 2018 2020
(c) 1990-2019
SWOOSH
Pressure (hPa)
1990 1992 1994 1996 1998 2000 2002 2004 2006 2008 2010 2012 2014 2016 2018 2020
-0.35 -0.3 -0.25 -0.2 -0.15 -0.1 -0.05 0 0.05 0.1 0.15 0.2 0.25 0.3 0.35

205

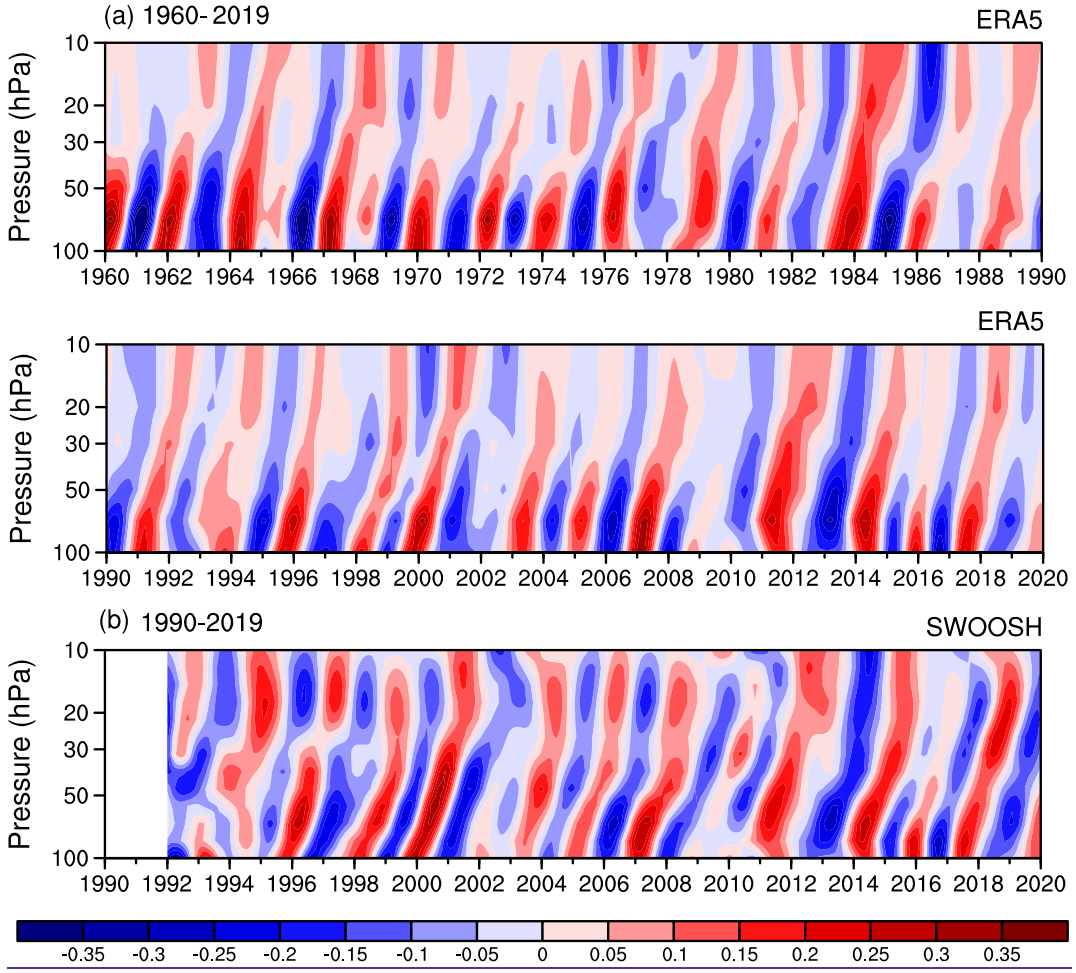

Figure ~~1~~2. (a~~,~~ ~~b~~) Temporal variations of ~~water vapor~~WV anomalies ~~(units: ppm)~~ averaged over the equator (5°S–5°N) with removed linear trends in the tropical stratosphere from 1960–2019 for ERA5 reanalysis (mass mixing ratio, units: ppm). (~~e~~b) W~~ater vapor~~V anomalies ~~(units: ppm)~~ from 1990–2019 for SWOOSH data (mass mixing ratio, units: ppm). The anomalies are filtered by applying a 15–60-month Butterworth bandpass filter.

Figure ~~2~~ 3 shows the zonal mean zonal wind and temperature anomalies in the tropical stratosphere. The zonal mean zonal wind anomalies in the tropical stratosphere show obvious QBO variations and propagate downward from 5 hPa to the lowermost stratosphere. The amplitude of zonal winds is relatively stable above 15 m/s at 5–30 hPa, and the maximum central amplitude can exceed 20 m/s. Zonal mean zonal wind anomalies weaken rapidly from 50–100 hPa. Zonal winds alternate between the easterly and westerly most of the time, except for the disruption of the QBO westerly by the lower stratospheric easterly in 2016 (Coy et al., 2017; Wang et al., 2023).

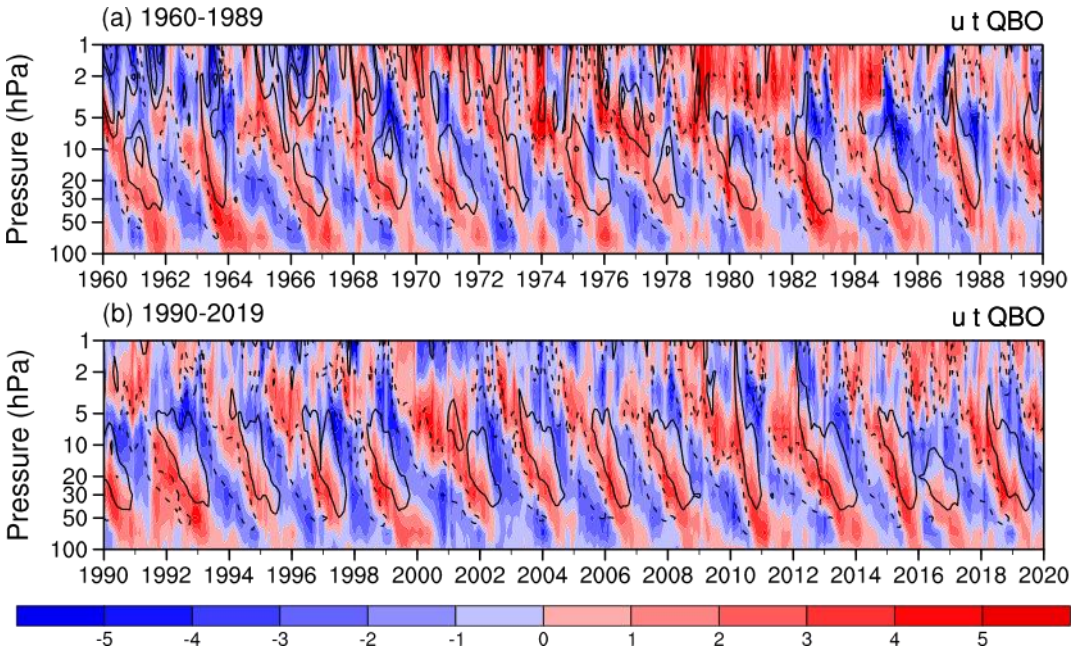

Figure ~~2~~3. Temporal variations of zonal mean zonal wind anomalies (contours; units: m/s) and temperature anomalies (shadings; units: K) averaged over the equator (5°S–5°N) with removed linear trends in the tropical stratosphere from 1960–2019 for ERA5 reanalysis. The ~~zonal wind anomaly shows contour lines~~contours are shown at ±15 m/s and ±30 m/s.

Consistent with the zonal wind anomalies, temperature anomalies in the tropics also exhibit evident QBO variability, which gradually propagates downward to the lower stratosphere from 5 hPa. Thermal wind balance predicts that cold anomalies should lie underneath strong easterly winds and warm anomalies underneath westerly winds, and such an effect is clearly evident with peak temperature anomalies in regions of strongest shear as expected theoretically (Allen and Sherwood, 2008). The temperature anomalies can propagate downward to 100 hPa, and the temperature anomaly amplitude can exceed 3 K. Figure 4 shows the lagged correlation coefficients between the QBO index at 30 hPa and the WV at each level. The amplitude of the WV QBO at 100 hPa can exceed 0.2 ppm, and the peak value can reach 0.35 ppm. The amplitude of the WV QBO at 100 hPa lags behind the amplitude of the zonal wind QBO at 30 hPa by 5 to 7 months, and the lag correlation coefficient is up to 0.75 (Fig. 4a). The amplitude of the WV QBO at 30 hPa is merely 0.1 ppm, and its peak value can reach 0.2 ppm. The amplitude of the WV QBO lags behind the amplitude of the zonal wind QBO by 14 to 16 months, and the lag correlation coefficient ~~amounts to~~is maximized around 0.51 (Fig. 4b). According to the lag correlation coefficient between zonal wind on 30 hPa and WV at~~in~~ each layer, WV on the 100 hPa level was ~~most~~affected in about half a year. In contrast, the upper level WV is~~was~~ affected by QBO at~~for a~~ longer lags~~period~~, and the lag correlation coefficient decrease~~d~~s accordingly (Fig. 4c). Previous studies indicated that the cold point temperature determines the WV in the tropical lower stratosphere (Randel and~~&~~ Park, 2019), while the secondary circulation excited by the QBO regulates the WV transport in the middle stratosphere (Geller et al., 2002). Therefore, the relationship between the QBO and WV is more significant in the lower and middle stratosphere.

The zonal wind and water vapor anomalies at 70 hPa, 10 hPa and 2 hPa are calculated respectively to explore the corresponding relationship between the zonal mean zonal wind QBO and water vapor QBO. The zonal wind anomalies are positively correlated with the water vapor anomalies at 70 hPa (correlation coefficient, CC=0.51). Basically, an increase in water vapor in the lower stratosphere happens during the QBO westerly, and a decrease in water vapor in the lower stratosphere appears during the QBO easterly phase (Fig. 3a). Their correlation at 10 hPa is even larger than at 70 hPa, which suggests that the water vapor QBO is more robustly present in the middle stratosphere (CC=0.58, Fig. 3b). The zonal wind variation at 2 hPa shows weak QBO signal: the zonal wind variability is relatively chaotic (Fig. 3c). Previous studies indicated that the cold point temperature determines the water vapor in the tropical lower stratosphere (Randel & Park, 2019), while the secondary circulation excited by the QBO regulates the water vapor transport in the middle stratosphere (Geller et al., 2002). Therefore, the relationship between the QBO and water vapor is significant in the lower and middle stratosphere.the cold point temperature determines the tropical water vapor in the stratosphere (Randel and Park, 2019), and so this relationship between the QBO and water vapor is to be expected.

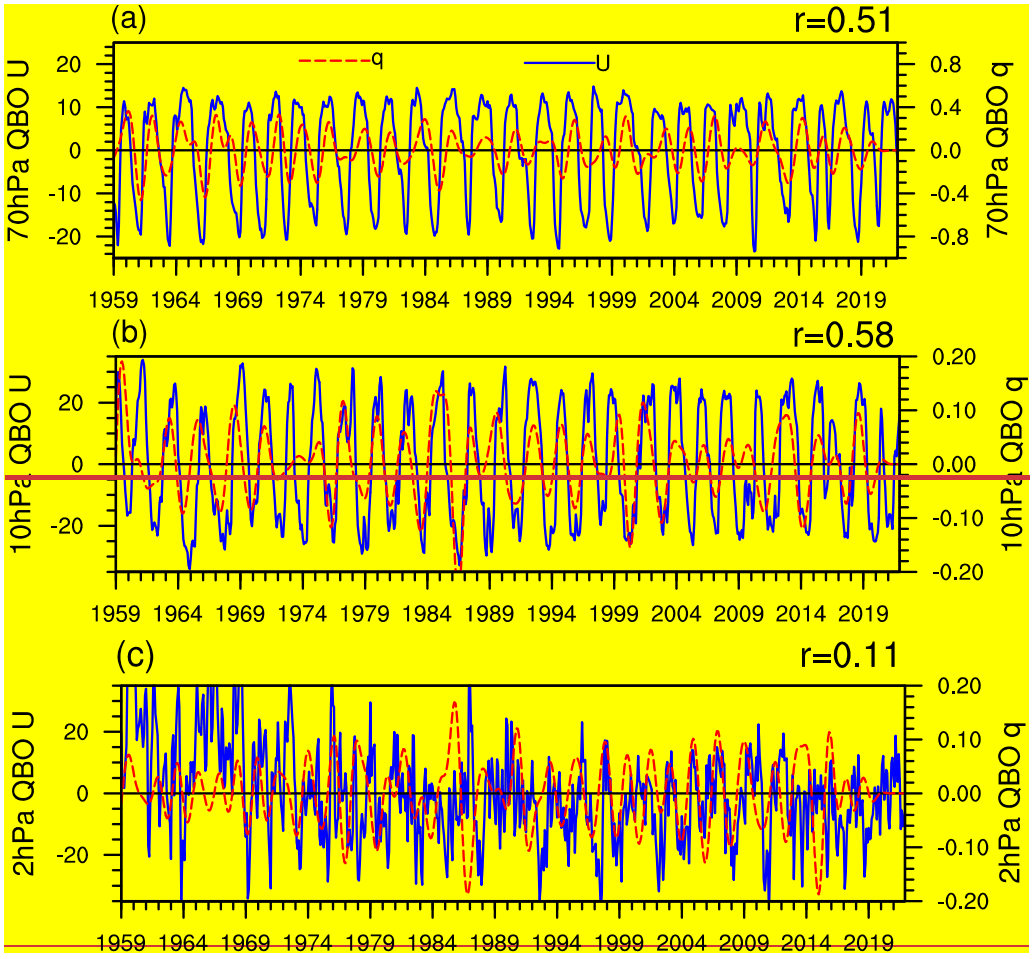
(a)
r=0.51
q
U
70hPa QBO U
70hPa QBO q
20
10
0
-10
-20
0.8
0.4
0.0
-0.4
-0.8
1959 1964 1969 1974 1979 1984 1989 1994 1999 2004 2009 2014 2019
(b)
r=0.58
10hPa QBO U
10hPa QBO q
20
0
-20
0.20
0.10
0.00
-0.10
-0.20
1959 1964 1969 1974 1979 1984 1989 1994 1999 2004 2009 2014 2019
(c)
r=0.11
2hPa QBO U
2hPa QBO q
20
0
-20
0.20
0.10
0.00
-0.10
-0.20
1959 1964 1969 1974 1979 1984 1989 1994 1999 2004 2009 2014 2019

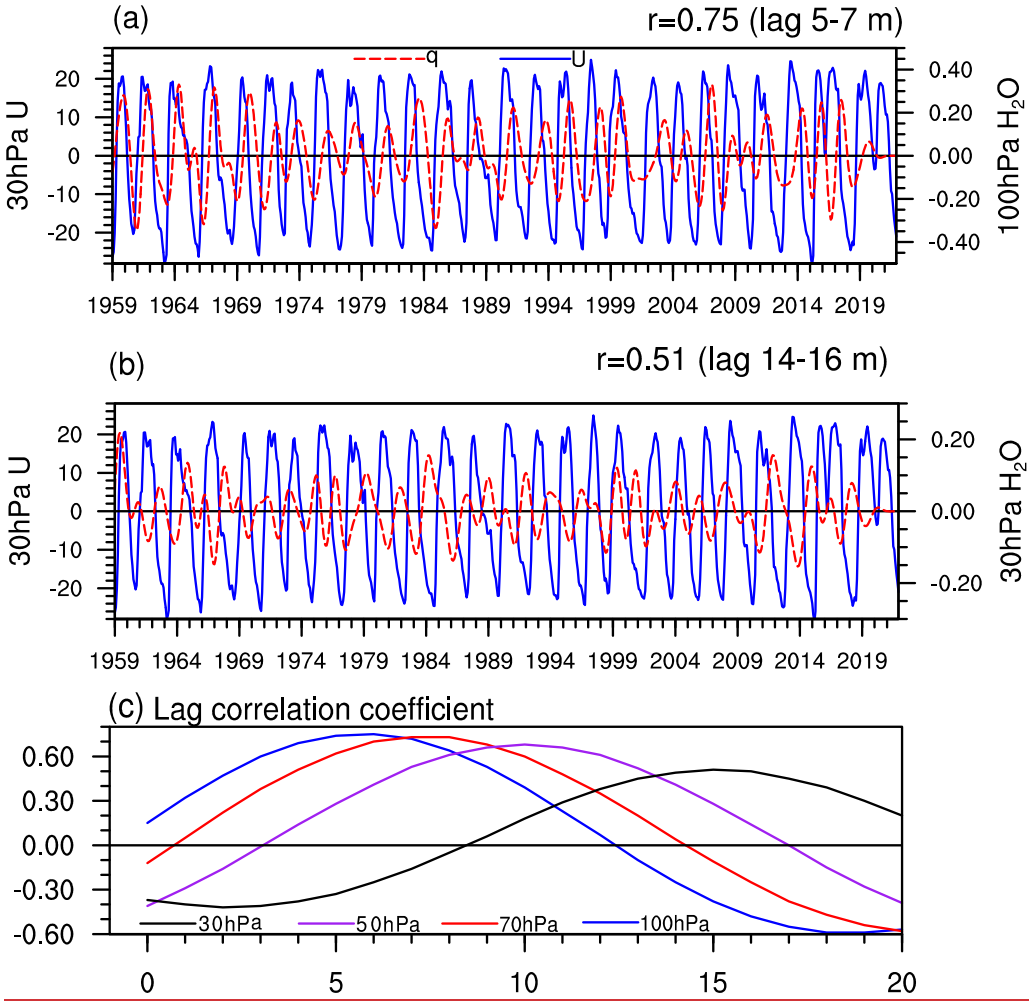

Figure~~. 34.~~ Zonal mean zonal wind anomalies at 30 hPa (unit: m/s) and ~~water vapor~~WV anomalies (unit: ppm) in the tropics (5°S–5°N) at (a) ~~70~~ 100 hPa, (b) ~~10~~ 30 hPa~~, and~~. (c) The lag correlation coefficient between 30 hPa zonal wind and WV lagging by different months~~2 hPa~~. W~~ater vapor~~V anomalies are bandpass filtered to focus on periodicities of 15–60 months, and zonal wind anomalies are linearly detrended.

4 Comparison of water vapor QBO between boreal winter and summer

a. Spatial distribution of ~~water vapor~~WV QBO

~~Figure 4 shows the distribution of water vapor~~WV ~~anomalies for different QBO phases in boreal winter and summer, respectively. Under the QBO westerly phase in the northern summer, the water vapor~~WV ~~anomaly is weak near the tropical tropopause at 100 hPa, while a larger negative anomaly center is observed at 50 hPa with the amplitude of around −0.1 ppm. (Fig. 4a). Under the QBO easterly phase in the northern summer, the water vapor~~WV ~~anomaly pattern is basically opposite to that of the QBO westerly phase. Specifically, tropical water vapor~~WV ~~near the tropopause is slightly reduced and at 30–70 hPa increased. This increase near 30–70hPa is displaced off the equator, towards the northern subtropics with the amplitude~~

~~of 0.04 ppm (Fig. 4b). Because the distribution of water vapor~~WV ~~anomalies in the westerly phase and the easterly phase in summer is almost opposite, the water vapor~~WV ~~difference between westerly and easterly QBO phase is consistent with the distribution of water vapor~~WV ~~anomalies in the westerly phase (Fig. 4c). It is also found that the tropopause in the tropics under the QBO westerly phase rises higher than that under the easterly phase.~~

~~Under the QBO westerly phase in the northern winter, a deep and strong positive vapor~~ WV ~~anomaly band appears between 50–150 hPa in the tropics, with the central amplitude exceeding 0.1 ppm. Water vapor~~V ~~decreases in the middle and upper stratosphere around 5–30 hPa in the tropics, in contrast with the moistening in the upper stratosphere around 1–2 hPa (Fig. 4d).~~

~~The distribution of water vapor~~WV ~~anomalies in the QBO easterly phase in the northern winter is nearly reversed to that in the QBO westerly phase. Water vapor~~V ~~around 50–150 hPa in the tropics and subtropics of both hemispheres decreases, with the maximum negative anomalies exceeding 0.1 ppm. Water vapor~~V ~~around 5–50 hPa in tropics increases, contrasted with the decrease around 2–5 hPa (Fig. 4e). The tropopause pressure of the QBO westerly phase in the tropics is about 5 hPa higher than that of the easterly phase.~~

~~In short, during~~ During both winter and summer, the influence of QBO on tropical stratospheric ~~water vapor~~WV entry is nearly symmetrical. Under the QBO westerly phase as an example, the distribution of tropical stratospheric ~~water vapor~~WV displays a sandwich structure with positive, negative and positive ~~water~~ WV anomalies from the lower to upper layers (Fig. S2). Further, the ~~water vapor~~WV anomalies in the lower stratosphere during winter ~~is~~ are stronger than during summer (Fig. S3).

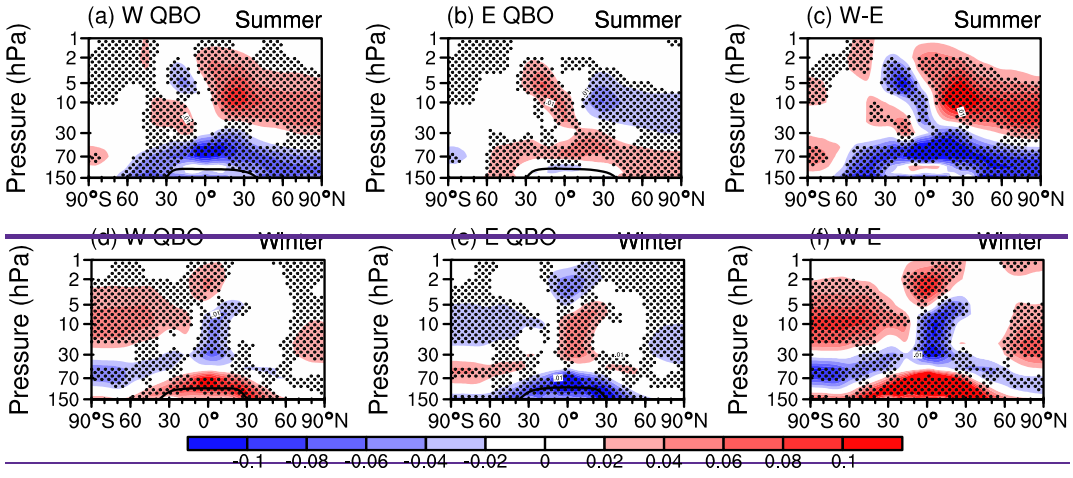

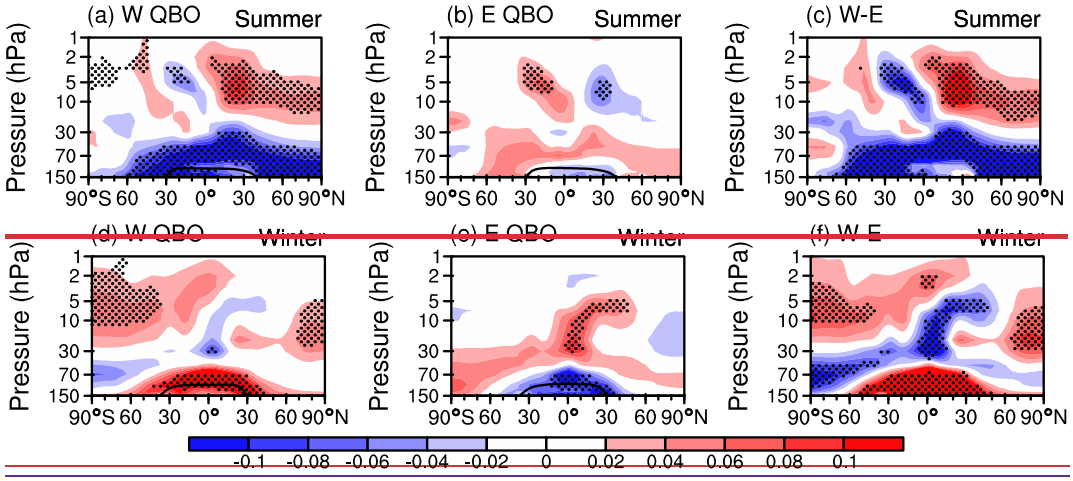

Figure. 4 Water vapor anomalies under different QBO phases in the northern winter and summer (mass mixing ratio, unit: ppm), respectively. Water vapor anomalies were bandpass filtered with the periods from 15–60 months, and t**The black line marks the tropopause for QBO composite. (a) Composite of QBO westerly in northern summer. (b) Composite of QBO easterly in northern summer. (c) The difference between a and b.(d–f) As in a–c, but for northern winter. Dots denote statistical significance at the 95% confidence level based on Student t-test.**

The primary source of stratospheric Swater vaporWV is tropical tropospheric water vaporWV entering the stratosphere. Figure 4 shows that the modulation effect of 30 hPa zonal wind QBO on 100 hPa WV reaches its maximum after a lag of half a year.Motivated by Figure 2 which shows a pronounced QBO temperature signal at 100hPa, Therefore, Figure 5 respectively shows the 100 hPa WV anomalies lagging by 6 months at different QBO phases in winter and summer. Figure 5 shows the tropical distribution of water vaporWV anomalies at 100 hPa. During the QBO westerly phase in the northern summer, water vaporWV in the tropics with a lag of 6 monthsin the tropical Pacific increases, and the center of the positive anomaly magnitude exceeds 0.04–12 ppm in the Indo-Pacific region (Fig. 5a). During the QBO easterly phase in the northern summer, water vaporWV with a lag of 6 months decreases with the maximum center of 0.06–16 ppm in the equatorial middle Pacific Indo-Pacific region (Fig. 5b). These summer anomalies are much smaller than the winter anomalies. Namely, during the QBO westerly phase in the northern winter, tropical water vaporWV with a lag of 6 months uniformly increases with the largest magnitude around 0.1–2 ppm in the Atlantic Ocean (Fig. 5c), and the dehydration with a lag of 6 months during the QBO easterly phase in the northern winter also peaks around -0.1ppm–2 ppm in the Atlantic Ocean (Fig. 5d). It is concluded that tThe amplitude of the water vaporWV response with a lag of 6 months at 100 hPa to the QBO forcing in winter is nearly 2–3 times of thatlarger than that to the QBO forcing in summer.

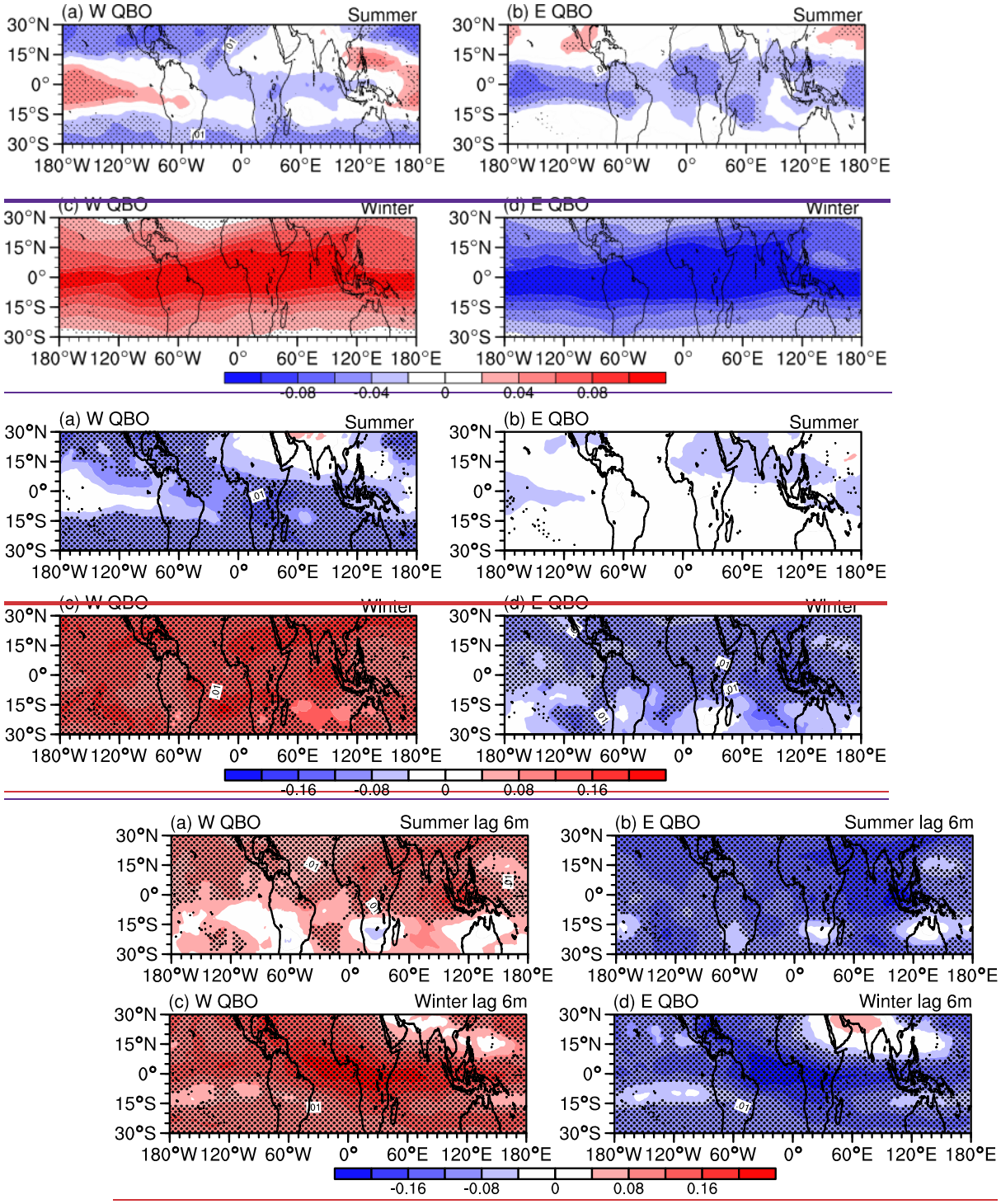

300

Figure~~.~~ 5. Distribution of ~~water vapor~~WV anomalies with a lag of 6 months at 100 hPa under different QBO phases in northern winter and summer (mass mixing ratio, unit: ppm), respectively. ~~Water vapor anomalies are bandpass filtered with the periods from~~

~~15–60 months.~~ **(a) Composite of QBO westerly in northern summer. (b) Composite of QBO easterly in northern summer. (c, d) As in (a, b) but for northern winter.**

b. Factors affecting the ~~water vapor~~WV distribution

Since the cold point temperature near the tropopause ~~regulate~~ regulates entry ~~water vapor~~WV (see the introduction), we now consider the temperature response to the QBO. Figure 6 shows the zonal mean temperature anomalies under different QBO phases in boreal summer and winter, respectively. It is found that the temperature anomalies in tropics–subtropics show a quadrupole pattern in both boreal summer (Fig. 6a, b) and winter (Fig. 6c, d), although the temperature quadrupole is positioned differently.

Under the QBO westerly phase in boreal summer, the tropical lower stratosphere around 30–100 hPa warms, while the middle and upper stratosphere around 5–30 hPa cool, as expected from thermal wind balance (Allen and Sherwood, 2008). The temperature anomalies in the Southern Hemisphere subtropics are nearly opposite to those in the tropics, with cold anomalies in the lower stratosphere and warm anomalies in the middle and upper stratosphere. A cold anomaly center with a magnitude of -1.5 K appears in the upper stratosphere over the Antarctic, corresponding to the strengthened polar vortex (Fig. 6a). Under the QBO easterly phase in boreal summer, the tropical lower stratosphere around 30–100 hPa cools, while the middle and high stratosphere around 5–30 hPa warms. The temperature anomalies in the Southern Hemisphere subtropics are opposite to those in the tropics, with warm anomalies in the lower stratosphere and cold anomalies in the middle and upper stratosphere. A cold anomaly center of ~4 K appears in the upper stratosphere over the Antarctic, corresponding to the weakening of the polar vortex (Fig. 6b).

Under the westerly QBO phase in boreal winter, the tropical lower stratosphere around 30–100 hPa is anomalously warm, and the middle stratosphere around 5–30 hPa is anomalously cold. The Northern Hemisphere subtropics are controlled by warm anomalies around 10–70 hPa and cold anomalies above. The upper stratosphere over the Arctic is anomalously warm, and the middle and lower stratosphere ~~is~~ are anomalously cold, corresponding to a strengthened Arctic polar vortex (Fig. 6c). Under the easterly phase in boreal winter, the lower stratosphere in the tropics is anomalously cold, and the middle and upper stratosphere around 10–30 hPa is anomalously warm. The Northern Hemisphere subtropics at around 10–30 hPa cool, and the stratopause is covered by warm anomalies. The Arctic stratopause is covered by cold anomalies, and the middle and lower stratosphere ~~is~~ are dominated by warm anomalies, corresponding to the weakening of the polar vortex (Fig. 6d).

By analyzing the stratospheric temperature anomalies at different QBO phases, it can be found that only the cold temperature at the bottom of the tropical stratosphere can affect the change of SWV, while the temperature change in the middle and upper stratosphere does not directly alter the ~~water vapor~~WV content.

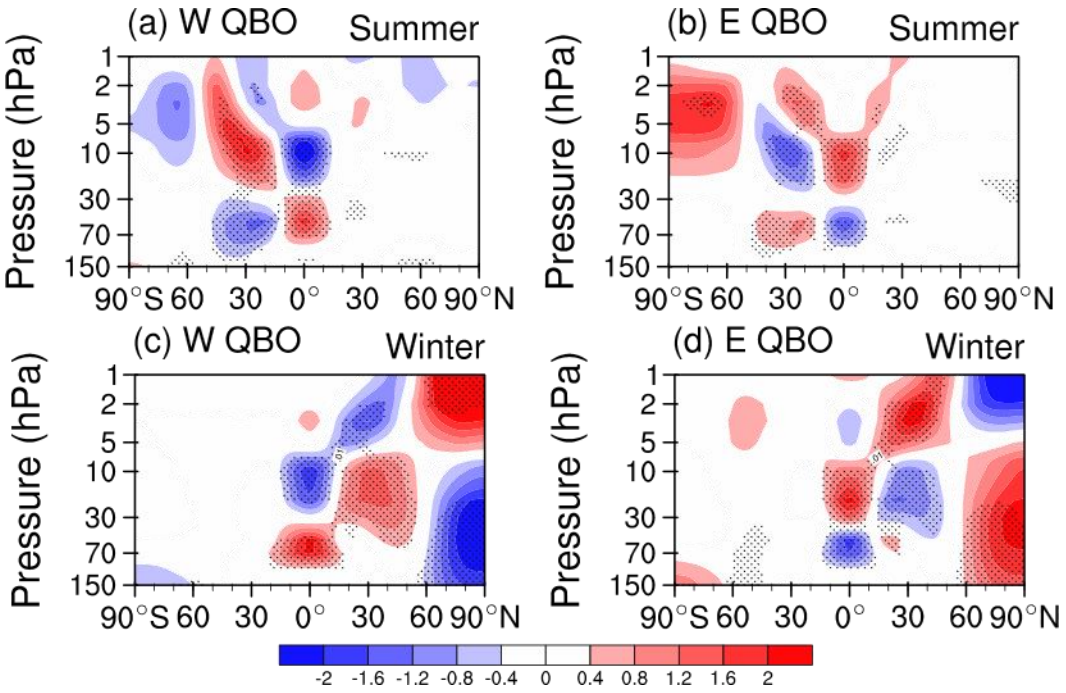

Figure~~.~~ 6. Zonal mean temperature anomalies under different QBO phases in northern winter and summer (unit: K), respectively. (a) Temperature anomalies during the QBO westerly phase in the northern summer. (b) Temperature anomalies during the QBO easterly phase in the northern summer. (c, d) As in a, b but for temperature anomalies for the northern winter. Dots mark the composite anomalies at the 95% confidence level.

The temperature near the tropopause and in the lower stratosphere significantly affects the distribution of WV entering the stratosphere especially in the tropics (Garfinkel et al., 2013, 2021; Ueyama et al., 2016). Comparing the temperature anomaly distribution in boreal winter versus summer, the coverage and amplitude of tropical temperature anomalies are very different: the lower stratospheric temperature variations associated with QBO in the tropics are much stronger in winter than in summer (Fig. S4). This is consistent with the discovery by Tegtmeier et al. (2020) that the QBO temperature amplitude is stronger in winter than in summer. Previous studies have shown that deep convection produces warming in the upper troposphere and cooling near the cold point tropopause (Gettelman and Birner, 2007; Kim et al., 2018; Muhsin et al., 2018). The QBO modulating the temperature signal on the southern side of the South Asian monsoon (i.e., the Indo-Pacific Warm Pool region) in July and August is related to the changes in equatorial clouds, which in turn affect the WV distribution in the upper troposphere and lower stratosphere of this region (Pena-Ortiz et al., 2024). The OLR anomalies add extra warm anomalies during the QBO westerly phase in the northern winter and cold anomalies during the QBO easterly phase in the northern winter, which increases the temperature difference between the easterly and westerly QBO phases, but this effect is relatively weak in the northern summer (Fig. S5).

As the influence of the QBO signal gradually propagates to lower layers, the temperature anomaly with a lag of 6 months at 100 hPa is shown in Figure 7. Under the QBO westerly phase in the northern summer, warm anomalies are distributed in a band-like pattern in the equatorial region, with the warmest point in the Indo-Pacific Warm Pool reaching 0.45 K (Fig. 7a).

Under the QBO easterly phase in the northern summer, the cold anomalies occurred in the equatorial region, and the cold center in the Indo-Pacific Warm Pool was -0.45 K (Fig. 7b). Under the QBO westerly phase in the northern winter, the range of warm anomalies in the equatorial region is wider, with the anomaly amplitude of ~0.6 K in the Atlantic Ocean and Africa (Fig. 7c). Under the QBO easterly phase in the northern winter, cold anomalies occur with a center of ~0.45 K in the Atlantic Ocean (Fig. 7d). The 30 hPa QBO affects the 100 hPa temperature amplitude half a year later, which in turn influences the WV entering the stratosphere. The QBO delayed impact in the northern winter is still stronger than that in summer.

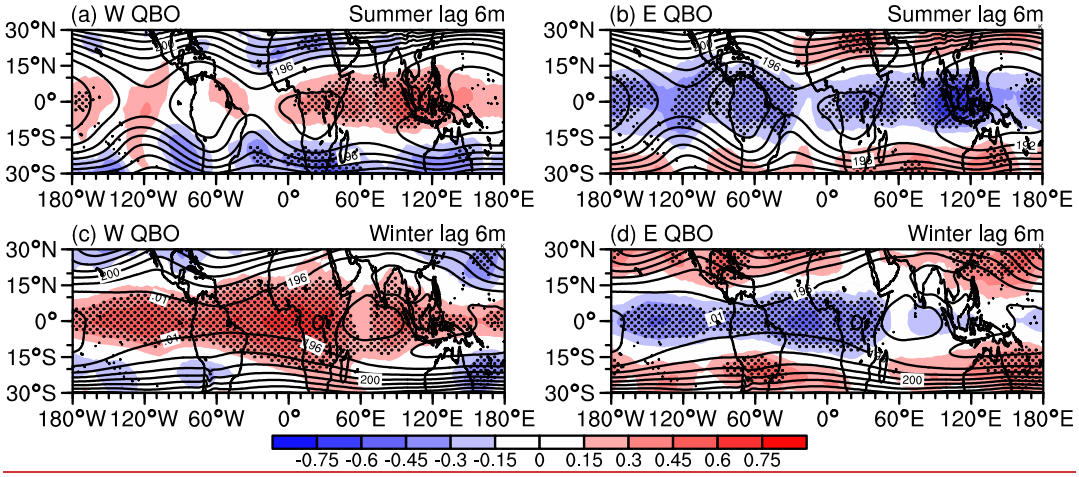

Figure 7. Temperature anomalies with a lag of 6 months at 100 hPa under different QBO phases in northern winter and summer (shadings; unit: K), respectively. (a) Temperature anomalies during the QBO westerly phase in the northern summer. (b) Temperature anomalies during the QBO easterly phase in the northern summer. (c, d) As in a, b but for temperature anomalies following the QBO in the northern winter. Contours show the temperature climatology in winter and summer (contour interval: 2), and dots mark the composite anomalies at the 95% confidence level.

The Brewer-Dobson (BD) circulation in the stratosphere can directly affect the transport of ~~water vapor~~WV from the tropical troposphere to the stratosphere (Holton et al. 1995; Butchart 2014; Keeble et al. 2021). The BD circulation also affects tropopause temperature in the tropics, which in turn affects ~~water vapor~~WV entering the stratosphere (Abalos et al., 2021; Butchart, 2014; Hardiman et al., 2014). Figure ~~7~~8 shows the BD circulation anomalies for different QBO phases in the northern winter and summer. The QBO-related secondary circulation anomalies are only evident in the winter hemisphere (i.e., the Southern Hemisphere in boreal summer and Northern Hemisphere in boreal winter), mainly due to enhanced active planetary waves at midlatitudes in the winter hemisphere.

Under the QBO westerly phase in northern summer, anomalous strong upwelling appears in the lower stratosphere over the Southern Hemisphere subtropics, accompanied ~~with~~ by anomalous strong downwelling in the tropics. As a consequence, a clockwise secondary circulation cell appears in the lower stratosphere. The residual circulation anomaly pattern in the middle and upper stratosphere is reversed: anomalous rising motion over the tropics and sinking over the Southern Hemisphere subtropics region (Fig. ~~7a~~8a). Under the easterly phase in boreal summer, the residual circulation anomalies show ascent in the tropical lower stratosphere and descent in the lower stratosphere of the Southern Hemisphere subtropics, resulting in a

counterclockwise secondary circulation cell in the lower stratosphere. In the middle stratosphere, the residual circulation anomalies show descent in the tropics and ascent in the subtropics, resulting in a clockwise circulation (Fig. ~~7b~~8b).

Under the westerly phase of the QBO in northern winter, the lower stratospheric residual circulation sinks in the tropics and rises in the subtropics. The middle stratospheric residual circulation rises in the tropics and sinks in the Northern ~~Hemisphere~~ hemisphere subtropics (Fig. ~~7c~~8c). Under the QBO easterly phase in the northern winter, the lower stratosphere vertical residual velocity anomaly shows~~residual circulation~~ upwelling in the tropics and sinking in the Northern Hemisphere subtropics with the ascending branch in the tropics being stronger ~~with the rising branch in the tropics stronger than the sinking branch in the extratropics~~. The residual circulation in the middle stratosphere sinks in the tropics and rises in the Northern Hemisphere subtropics. The descent over the Arctic is strengthened in winter, corresponding to weakening of the polar vortex (Fig. ~~7d~~8d).

For all circumstances, the secondary circulation cell is consistent with the distribution of stratospheric temperature anomalies: downwelling leads to warm and upwelling leads to cold via adiabatic heating/cooling. Namely, when an air mass descends, it is compressed, its volume decreases, its internal energy increases, and its temperature rises. This phenomenon is called adiabatic heating. Conversely, during ascent, adiabatic cooling occurs. The anomalous secondary circulation ~~does~~ not only ~~lead~~ leads to the advection of ~~water vapor~~WV in the tropical stratosphere~~,~~, but also affects the tropopause cold point temperature.

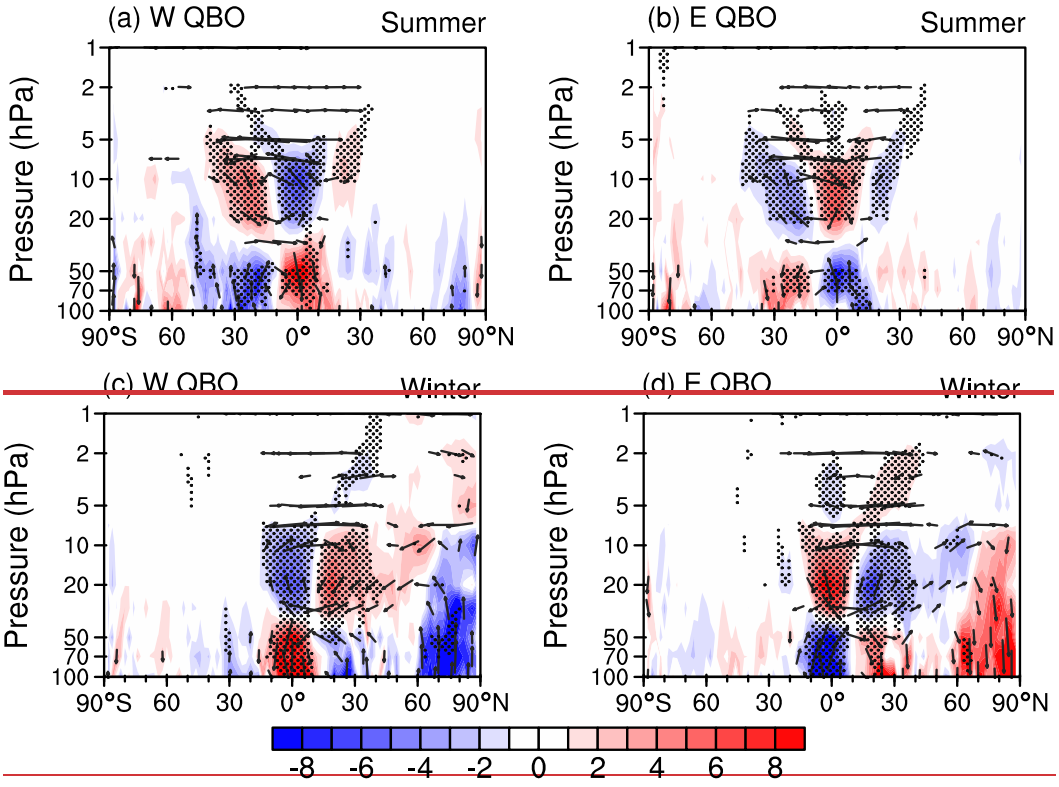

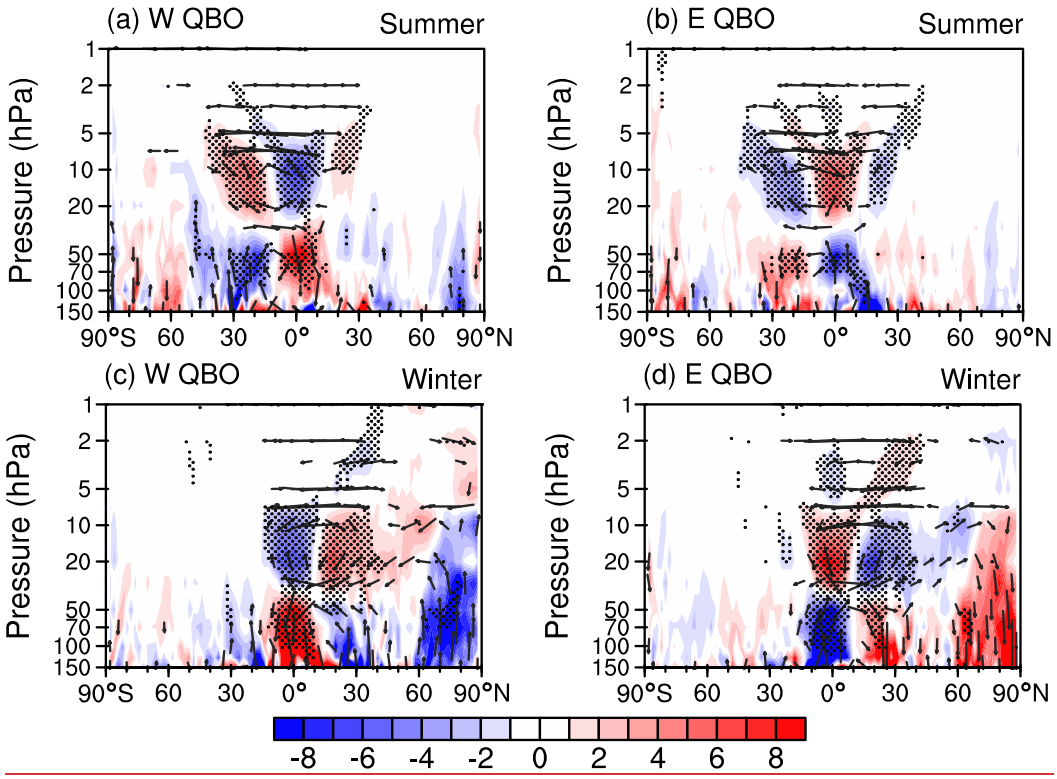

Figure~~.~~ ~~7~~8. (a) Residual circulation anomalies during the QBO westerly phase in the northern summer (units: 10^{-5} Pa/s). (b) Residual circulation anomalies during the QBO easterly phase in the northern summer (units: 10^{-5} Pa/s). (c, d) As in a, b but for residual circulation anomalies for the northern winter (units: 10^{-5} Pa/s). Dots mark the composite vertical residual velocity anomalies at the 95% confidence level. The shading is the vertical component of the residual velocities ~~(units: 10^{-5} Pa/s)~~.

~~The temperature near the tropopause and in the lower stratosphere significantly affects the distribution of water vapor entering the stratosphere especially in the tropics (Garfinkel et al., 2013, 2021; Ueyama et al., 2016). Figure 8 shows the temperature and its anomalies at 100 hPa associated with the QBO variability in the northern winter and summer, respectively. Under the QBO westerly phase in the northern summer, the temperature anomalies in tropics are weak and insignificant (Fig. 8a). Under the QBO easterly phase in the northern summer, significant cold anomalies occur in the tropical Indian Ocean and broad part of tropical Pacific (Fig. 8b). Under the QBO westerly phase in the northern winter, warm anomalies appear in the tropical climatological coldest centers with the anomaly amplitude of ~ 0.45 K (Fig. 8c), while cold anomalies appear under the QBO easterly phase in the northern winter with comparable anomaly amplitude (Fig. 8d). Warm temperature anomalies over the equator are accompanied with anomalously more water vapor, while cold temperature anomalies are accompanied with anomalously less water vapor. This well explains the distribution of water vapor anomalies in the lower stratosphere in the tropics under both westerly and easterly phases of QBO. Comparing the temperature anomaly distribution in boreal winter versus summer, the coverage and amplitude of tropical temperature anomalies are very different: the lower stratospheric temperature variations associated with QBO in the tropics are much stronger in winter than in summer. This is consistent with~~

the discovery by Tegtmeier et al. (2020) that the QBO temperature amplitude is stronger in winter than in summer. As a result, the water vapor amplitude at the bottom of the tropical stratosphere is stronger in winter and weaker in summer.

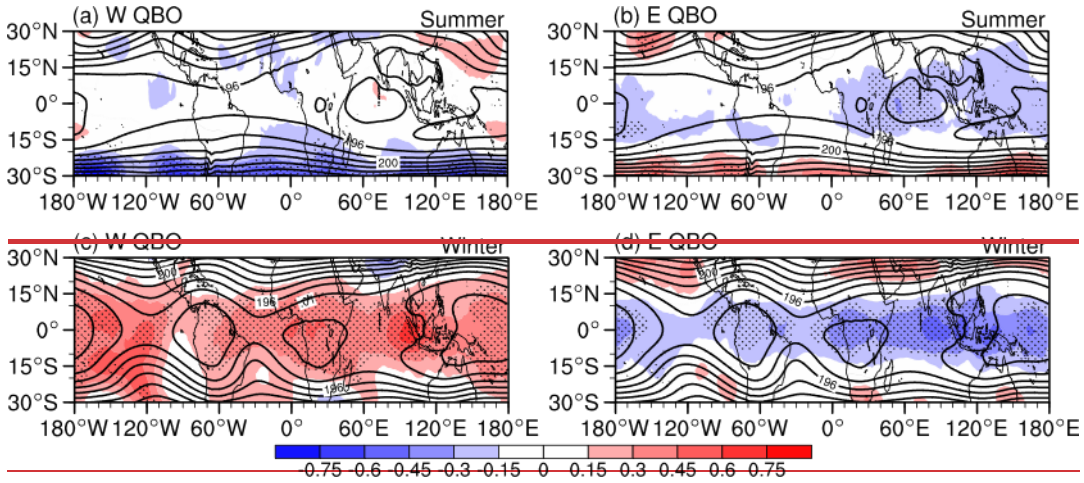

Figure. 8 Temperature anomalies at 100 hPa under different QBO phases in northern winter and summer (shadings; unit: K), respectively. (a) Temperature anomalies during the QBO westerly phase in the northern summer. (b) Temperature anomalies during the QBO easterly phase in the northern summer. (c, d) As in a, b but for temperature anomalies for the northern winter. Contours show the temperature climatology in winter and summer (contour interval: 2), and dots mark the composite anomalies at the 95% confidence level.

Previous studies have shown that deep convection produces warming in the upper troposphere and cooling near the cold point tropopause (Gettelman and Birner, 2007; Kim et al., 2018; Muhsin et al., 2018). Due to higher sea surface temperatures (SSTs) in the Indo-Pacific region, the convection over this region is relatively active while the tropopause cold point temperature is relatively low (Fueglistaler et al., 2009). This combination suggests that the QBO might be able to influence convection in this region. The QBO modulating the temperature signal on the southern side of the South Asian monsoon (i.e., the Indo-Pacific Warm Pool region) in July and August is related to the changes in equatorial clouds, which in turn affects the water vapor distribution in the upper troposphere and lower stratosphere of this region (Pena-Ortiz et al., 2024). We now consider this possibility in Fig. 9. After using linear regression to eliminate the influence of ENSO on OLR, the OLR anomaly under QBO easterly and westerly phases was obtained. Under the QBO westerly phase in the northern summer, the outgoing longwave radiation (OLR) anomalies in the Indo-Pacific region are negative, indicating that the tropical deep convection is relatively active (Fig. 9a), which is beneficial to decrease the tropopause cold point temperature in tropics. Under the QBO easterly phase in the northern summer, positive OLR anomalies prevail in the Indo-Pacific region, indicating relatively inactive convection (Fig. 9b). Under the QBO westerly phase in the northern winter, positive OLR anomaly in the Indo-Pacific region indicates that convective activity is inhibited (Fig. 9c). Under the QBO easterly phase in the northern winter, OLR anomalies in the Indo-Pacific region are anomalously negative, indicating significant enhancement of convective activities (Fig. 9d). The OLR anomalies add extra warm anomalies during the QBO westerly phase in the northern winter and cold anomalies during the QBO easterly phase in the northern winter (Fig. 8c, d), which increases the temperature difference between the easterly and westerly QBO phases. This effect is relatively weak in the northern summer (Fig. 8a, b).

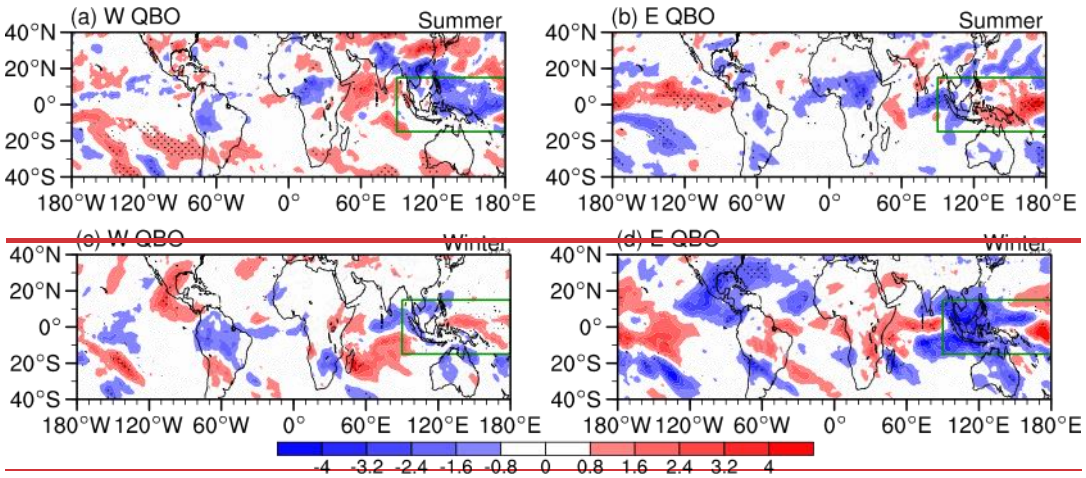

~~Figure. 9 Outgoing longwave radiation (OLR) anomalies under different QBO phases in northern winter and summer (unit: W m^{-2}), respectively. (a) OLR anomalies during the QBO westerly phase in the northern summer. (b) OLR anomalies during the QBO easterly phase in the northern summer. (c, d) As in a, b but for temperature~~ OLR ~~anomalies for the northern winter. Dots mark the composite anomalies at the 95% confidence level.~~

The transformed Eulerian-Mean (TEM) tracer continuity equation is used to quantify the balance of ~~stratospheric water vapor~~SWV associated with the QBO. Since the ~~water vapor~~WV QBO is stronger in northern winter, the TEM diagnosis for the northern winter is shown in ~~Fig.~~ Figure ~~10~~9. Under the QBO westerly phase, the tropical ~~water vapor~~WV shows a positive tendency in the lower stratosphere and a negative tendency in the middle stratosphere (Fig. ~~10a~~9a), explaining the ~~water vapor~~WV anomalies ~~(Fig. 4d)~~. The first two terms on the right side of Eq. 1 are the mean transport of ~~water vapor~~WV by the residual circulation (Fig. ~~10b~~9b). The change of mean advection of ~~water vapor~~WV is basically consistent with the tendency of ~~water vapor~~WV in the tropical region. Positive and negative anomalies are observed at the lower and upper stratosphere, respectively. However, in the tropical lower stratosphere, the positive anomaly of the mean advection is smaller than that of the ~~water vapor~~WV tendency (Fig.~~10~~9b). In the tropics, the meridional and the vertical mean advections together constitute the mean advection term (Fig.S~~2~~6). Namely, the residual circulation explains partially the ~~water vapor~~WV variation in the tropical stratosphere. The transport of WV by the eddy advection occurs mainly in the northern hemisphere (Fig.~~10~~9c) and is counterbalanced by the residual term (Fig.~~10~~9d). It is worth noting that at the bottom of the tropical stratosphere, the residual term generates positive WV anomalies, associated with increase in the cold point temperature of the tropical tropopause under the QBO westerly phase (Fig.~~10~~9d). The tendency ~~and~~, mean advection and eddy advection ~~transport~~ of ~~water vapor~~WV during the QBO easterly phase in the northern winter (Fig. ~~10e~~9e, ~~f~~,g) are generally opposite to those during the QBO westerly phase. The residual item also exhibits negative ~~water vapor~~WV anomalies in the tropical lower stratosphere (Fig. ~~10h~~9h). Through the above analysis, it can be found that the SWV changes in the tropics caused by QBO are mainly produced by the mean advection term by the residual circulation, and the cold temperature changes resulting from the residual term at the bottom of the tropical stratosphere also contributes to SWV variations.

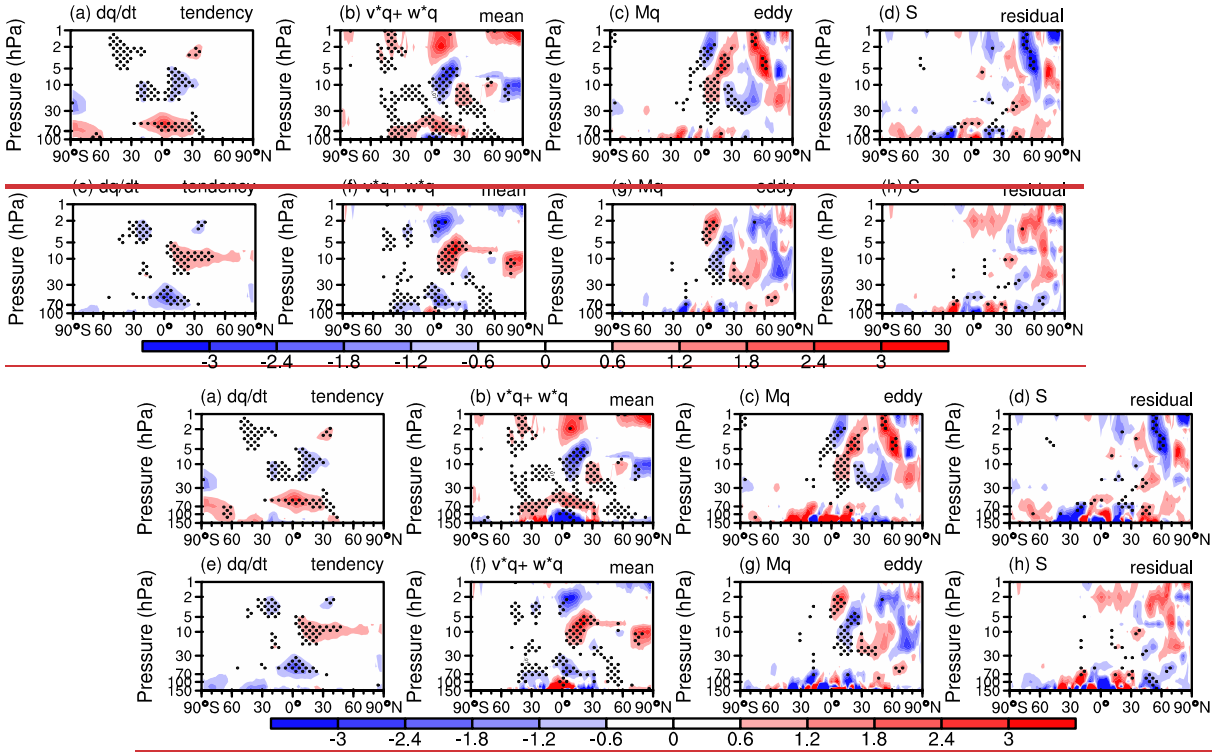

Figure~~. 10~~9. Diagnosis of the transformed Eulerian-Mean (TEM) tracer continuity equation in the northern winter. (a) W~~ater vapor~~V tendency during the QBO westerly phase (units: ppb day^{-1}). (b) The mean advection of ~~water vapor~~WV during the QBO westerly phase (ppb day^{-1}). (c) The eddy transport of ~~water vapor~~WV during the QBO westerly phase (ppb day^{-1}). (d) The residual term of ~~water vapor~~WV during the QBO westerly phase (ppb day^{-1}). (e-h) The same as in a-d but for QBO easterly phase.

5 Water vapor QBO in CMIP6 models

Since ~~stratospheric water vapor~~SWV has important climatic effects, evaluation of the simulated ~~water vapor~~WV QBO by CMIP6 models is helpful in diagnosing how to improve the performance of the models (Keeble et al., 2021; Ziskin ~~Ziv~~ et al., 2022). Figure ~~11~~ 10 shows the simulation of S~~stratospheric water vapor~~WV QBO from 18 CMIP6 high-top models. Given that the ~~water vapor~~WV QBO signal in the CMIP6 models is generally weak, different color scales are used in Figures ~~1~~2 and 1~~1~~0 to display the signal more clearly. Comparing the simulated ~~water vapor~~WV QBO from CMIP6 models with the ERA5 reanalysis data (Fig. ~~1~~2, Fig. S1), 11 models (ACCESS-CM2, AWI-CM-1-1-MR, CESM2-WACCM-FV2, CESM2-WACCM, GFDL-ESM4, HadGEM3-GC31-LL, HadGEM3-GC31-MM, MIROC6, MPI-ESM1-2-HR, MRI-ESM2.0, and UKESM1-0-LL) can effectively simulate the QBO variation of ~~water vapor~~WV in the middle and lower stratosphere (10–100 hPa). The ~~water vapor~~WV anomalies show continuous upward propagation from the lower to upper stratosphere in these models. The ~~water vapor~~WV QBO in MIROC6 only propagates to 20 hPa, which is relatively shallow compared to the ERA5 reanalysis. The ~~water vapor~~WV QBO in the upper stratosphere around 1–5 hPa is simulated in eight models (AWI-CM-1-1-MR, CESM2-WACCM-FV2, CESM2-WACCM, CNRM-CM6-1, GFDL-ESM4, MIROC6, MPI-ESM1-2-HR, and UKESM1-0-LL, Fig.

S7). ERA5 and SWOOSH show a change in the QBO-related anomaly pattern around 10 hPa. Below 10 hPa there is a tape-recorder of upward propagating anomalies, whereas above 10 hPa there seems to be a more direct effect of transport modulated by the QBO-induced secondary circulation (Fig. S1). This change in anomaly pattern is only visible in a few models (e.g. CESM2-WACCM, UKESM1-0-LL). Differences in the height coverage of the ~~water vapor~~WV QBO prevail among CMIP6 models.

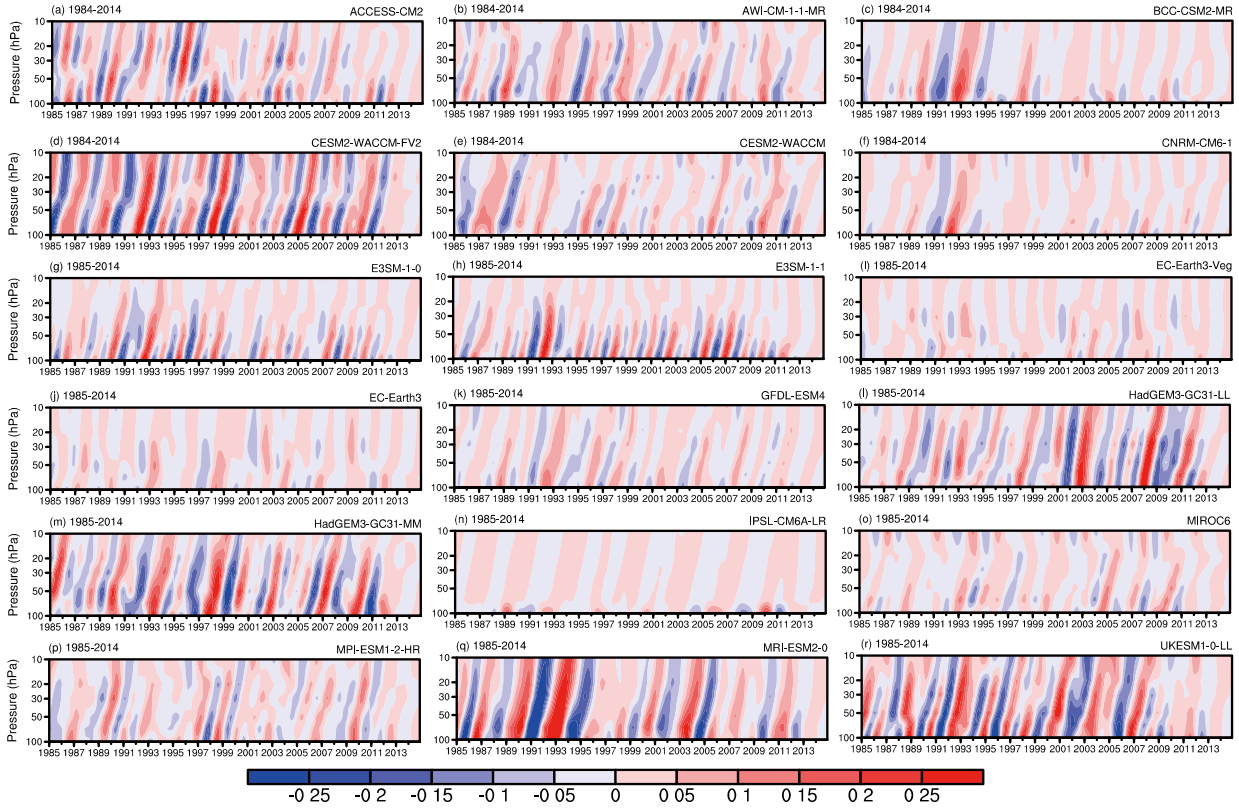

Figure~~.~~ ~~11~~10. Historical simulation of ~~water vapor~~WV QBO for (a–r) 18 CMIP6 models. ~~Stratospheric water vapor~~SWV anomalies in the tropics (5°S–5°N) during 1985–2014 have been bandpass filtered to focus on periodicities between 15 and 60 months (mass mixing ratio, units: ppm).

The spatial pattern of the ~~water vapor~~WV QBO in northern summer is shown in Fig. ~~12~~ S8 for 18 CMIP6 models, respectively. In general, models that simulate a tape recorder effect in Fig. ~~11~~ 10 also simulate a more realistic latitude vs. height response in Fig. ~~12~~S5. The relative abilities of each model are quantified in Table 1, which calculates the spatial correlation coefficients of ~~water vapor~~WV at 100-1 hPa and 30°S - 30°N between ERA5 reanalysis and CMIP6 models. It is shown that the spatial correlation coefficient between seven models and ERA5 exceeds 0.5 (AWI-CM-1-1-MR, CESM2-WACCM-FV2, E3SM-1-1, EC-Earth3, MIROC6-CM2, MPI-ESM1-2-HR, MRI-ESM2-0), and they can simulate negative ~~water vapor~~WV anomalies in the tropical lower stratosphere under the QBO westerly phase and positive anomalies under the QBO easterly phase in summer. Among the seven high-skill models, the ~~water vapor~~WV anomalies in CESM2-WACCM-FV2 are the largest, while the ~~water vapor~~WV anomalies in EC-Earth3 are the weakest. The ~~water vapor~~WV correlation coefficient between models

(CESM2-WACCM-FV2 and MRI-ESM2-0) and the ERA5 reanalysis exceeds 0.8~~The water vapor distribution simulated by CESM2-WACCM-FV2 and MRI-ESM2-0 models under different QBO phases in northern summer agrees most with ERA5~~ (Table 1), but even for those two models the biases relative to ERA5 is not little.

Figure ~~13~~ S9 shows the simulation of ~~water vapor~~WV anomalies under different QBO phases by 18 CMIP6 high-top models in northern winter. Table 1 also calculates the spatial correlation coefficients of ~~water vapor~~WV at 100-1 hPa and 30°S-30°N between ERA5 reanalysis and CMIP6 models. It can be observed that the ~~water vapor~~WV QBO in boreal winter is more difficult to reproduce than in summer for most models. Only five models (ACCESS-CM2, AWI-CM-1-1-MR, BCC-CSM2-MR, HadGEM3-GC31-MM, IPSL-CM6A-LR) can simulate the positive ~~water vapor~~WV anomalies in the tropical lower stratosphere under the westerly QBO phase and the negative anomalies under the easterly QBO phase in winter. The spatial correlation coefficient between BCC-CSM2-MR and ERA5 reanalysis is the highest in the tropics (0.82).

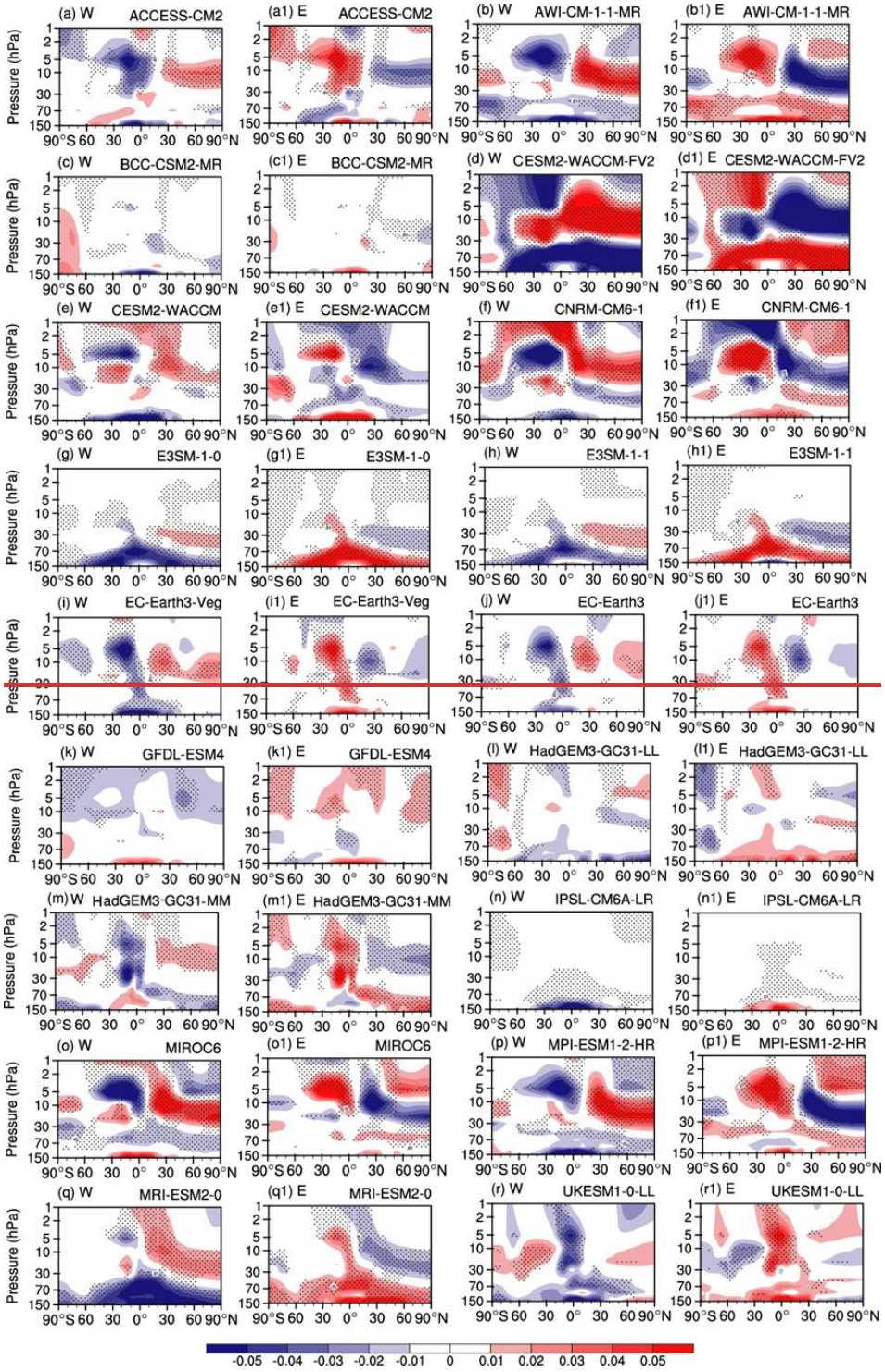

Figure. 12 As in Figure. 4 but for composite water vapor anomalies under different QBO phases in the northern summer (unit: ppm), respectively, for 18 CMIP6 models.

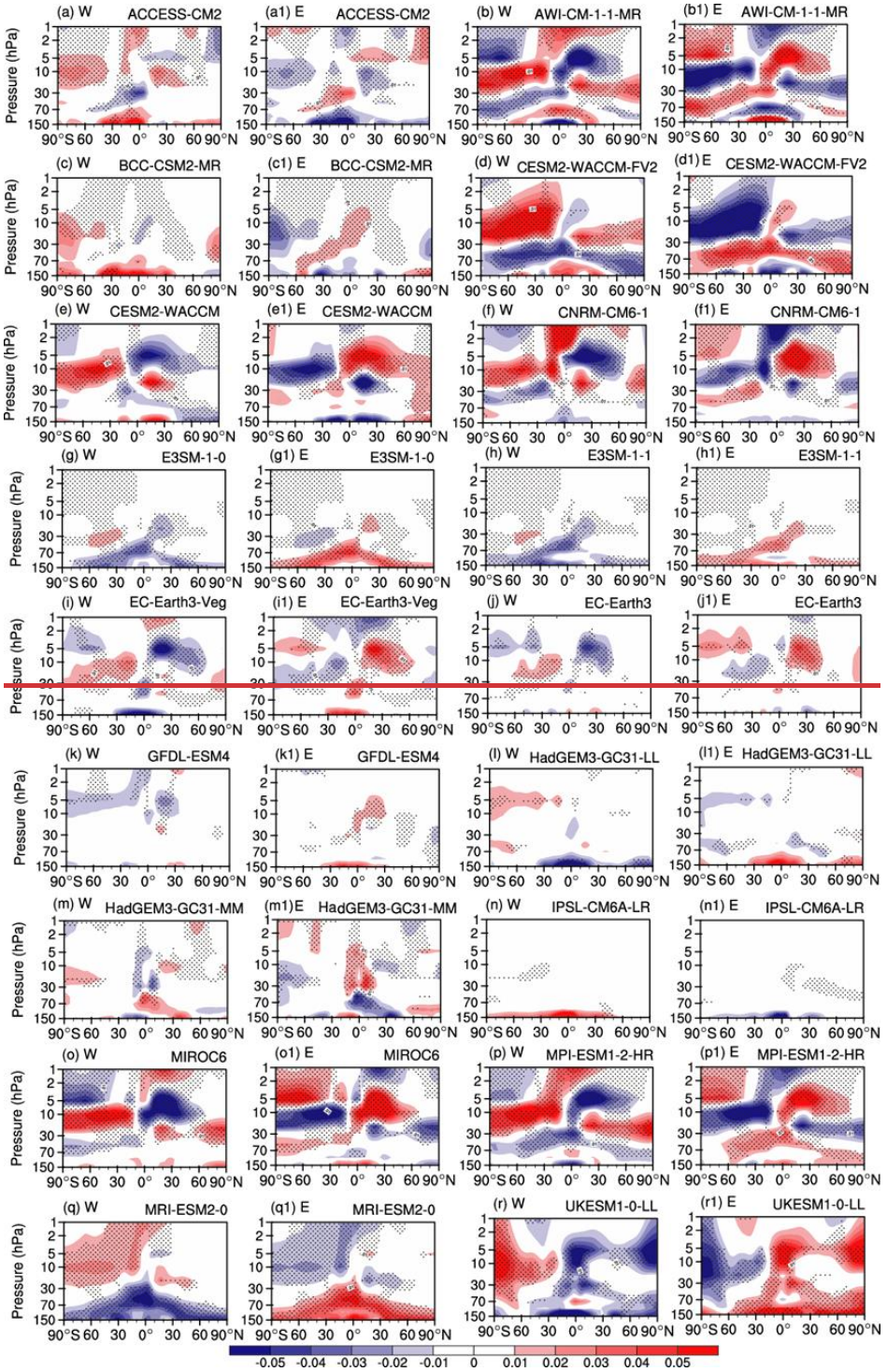

~~Figure. 13 As in Figure. 12 but for composite water vapor anomalies under different QBO phases in the northern winter (unit: ppm), respectively, for 18 CMIP6 models.~~

Most models struggle to simulate the contrast in ~~water vapor~~WV between winter and summer. Most models only simulate the winter or summer ~~water vapor~~WV QBO, and few models simulate the ~~water vapor~~WV QBO pattern in both seasons. Only one model (AWI CM-1-1-MR) can simulate the seasonal contrast in ~~water vapor~~WV distribution with the pattern correlation exceeding 0.5~~Only two models (AWI CM-1-1-MR and CESM2-WACCM-FV2) can simulate the seasonal contrast in water vapor distribution with the pattern correlation exceeding 0.5~~, although the general ~~water vapor~~WV anomaly patterns show biases from the ERA5 reanalysis (Fig. 4S2).

Table 1 Pattern correlation between ERA5 reanalysis and CMIP6 models for WQBO minus EQBO ~~water vapor~~WV difference at 100-1hPa and 30°S-30°N.

CMIP6 model	Winter	Summer
ACCESS-CM2	0.56	0.02
AWI-CM-1-1-MR	0.57	0.56
BCC-CSM2-MR	0.82	0.36
CESM2-WACCM-FV2	0.29	0.87
CESM2-WACCM	0.08	0.34
CNRM-CM6-1	0.07	0.43
E3SM-1-0	-0.61	0.39
E3SM-1-1	-0.08	0.50
EC-Earth3-Veg	0.19	0.45
EC-Earth3	0.32	0.50
GFDL-ESM4	0.45	-0.18
HadGEM3-GC31-LL	-0.42	0.09
HadGEM3-GC31-MM	0.67	0.20
IPSL-CM6A-LR	0.60	0.08
MIROC6-CM2	0.36	0.59
MPI-ESM1-2-HR	0.32	0.52
MRI-ESM2-0	-0.35	0.86
UKESM1-0-LL	0.31	0.23
MME	0.76	0.87

Previous work has suggested that models with a stronger QBO in the lower stratosphere are better capable of simulating its effect on entry ~~water vapor~~WV (Ziskin et al 2022), and we now consider this effect in these 18 models. Figure ~~14~~11 shows the scatter plots of QBO westerly phase minus easterly phase for the ~~50~~30 hPa zonal wind index and 70 hPa ~~water vapor~~WV

anomalies with a lag of 6 months in deep tropics among CMIP6 models. In the northern summer, the CMIP6 high-top models can simulate the positive correlation between the 30 hPa QBO index and WV lagging by six months at 70 hPa, with a multi-model correlation reaching 0.68 (p=0). Eight models simulate QBO index differences between easterly and westerly phases exceeding 30 m/s, which are comparable to the ERA5 QBO indices. However, the 70 hPa WV lagging by six months is less than half of that in ERA5 (Fig. 11a). In winter, CMIP6 models also capture the positive correlation between the QBO index and the 70 hPa WV lagging by six months, with a multi-model correlation coefficient of 0.54 (p=0.98).~~In summer, the 50 hPa QBO intensity simulated by the CMIP6 models is generally weaker than ERA5, and the QBO index intensity is generally negatively correlated with the water vapor response (Fig. 14a). In winter, the positive correlation between the 50 hPa QBO intensity and the 70 hPa water vapor response is not present among CMIP6 models.~~ Eight models show higher 30-hPa QBO index than that in ERA5, but only six of them exhibited WV anomalies around 0.1 ppm, with too-small WV amplitudes (Fig. 11b). Simulation performance is better in northern summer than in winter.

The pattern correlation in Table 1 is used as a criterion to select high-skill models. Specifically, the composites of 7 CMIP6 models (AWI-CM-1-1-MR, CESM2-WACCM-FV2, E3SM-1-1, EC-Earth3, MIROC6-CM2, MPI-ESM1-2-HR, MRI-ESM2-0) for summer QBO signals and 5 CMIP6 models (ACCESS-CM2, AWI-CM-1-1-MR, BCC-CSM2-MR, HadGEM3-GC31-MM, IPSL-CM6A-LR) for winter QBO signals are shown in Fig. ~~14~~S10. The spatial correlation coefficient between CMIP6 and ERA5 reanalysis reaches 0.87 for summer QBO signals. The ~~water vapor~~WV anomalies above 70 hPa are basically consistent with the ERA5 reanalysis (Fig. ~~14a~~S9a, b vs. Fig. 4~~a~~S2a, b). The spatial correlation coefficient of ~~water vapor~~WV between CMIP6 and ERA5 reanalysis is 0.76 for winter QBO signals. While these models capture the spatial pattern of the ~~water vapor~~WV anomalies, they struggle with the magnitude: the composite ~~water vapor~~WV anomaly magnitude from CMIP6 models is only half of that in the ERA5 reanalysis.

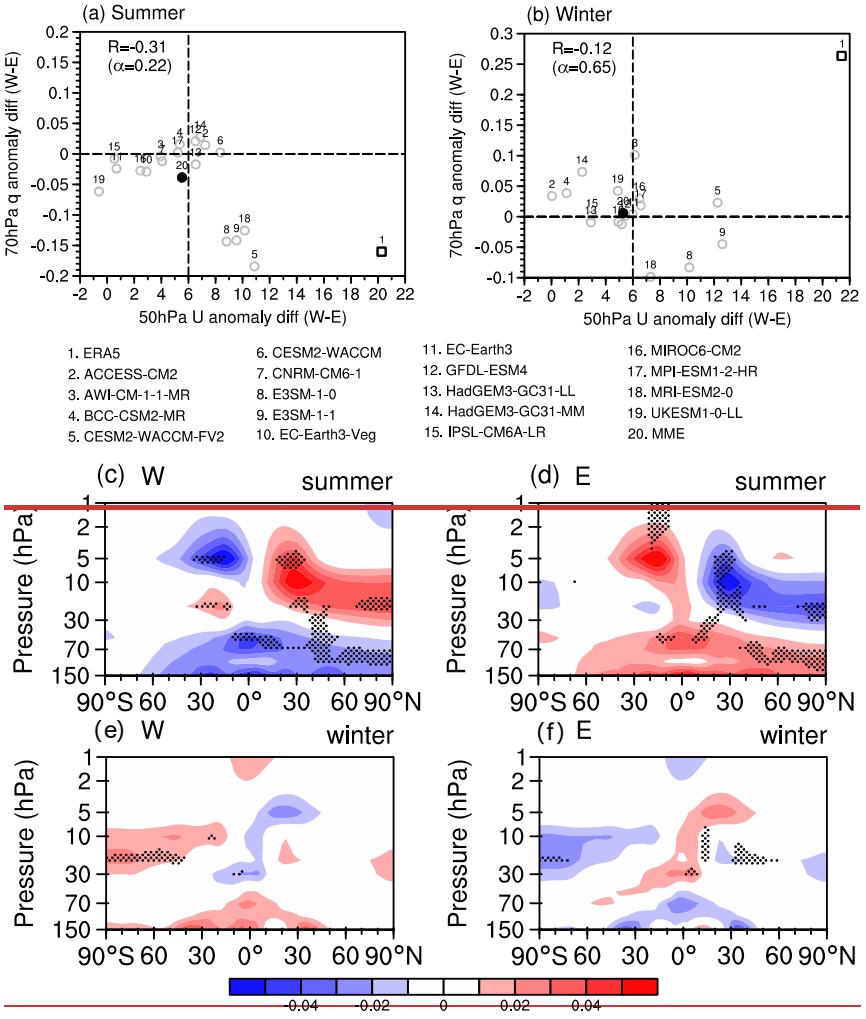
(a) Summer
R=-0.31
(α=0.22)
70hPa q anomaly diff (W-E)
50hPa U anomaly diff (W-E)
(b) Winter
R=-0.12
(α=0.65)
70hPa q anomaly diff (W-E)
50hPa U anomaly diff (W-E)
1. ERA5
2. ACCESS-CM2
3. AWI-CM-1-1-MR
4. BCC-CSM2-MR
5. CESM2-WACCM-FV2
6. CESM2-WACCM
7. CNRM-CM6-1
8. E3SM-1-0
9. E3SM-1-1
10. EC-Earth3-Veg
11. EC-Earth3
12. GFDL-ESM4
13. HadGEM3-GC31-LL
14. HadGEM3-GC31-MM
15. IPSL-CM6A-LR
16. MIROC6-CM2
17. MPI-ESM1-2-HR
18. MRI-ESM2-0
19. UKESM1-0-LL
20. MME
(c) W summer
(d) E summer
(e) W winter
(f) E winter
Pressure (hPa)
90°S 60 30 0° 30 60 90°N
-0.04 -0.02 0 0.02 0.04

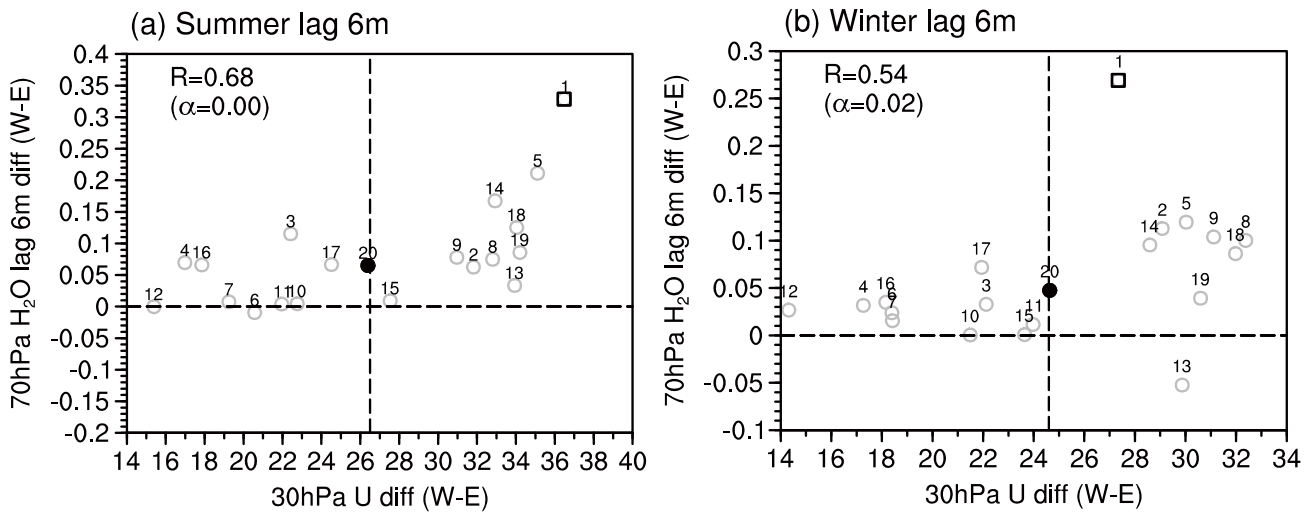

Figure~~.~~ ~~14~~11. Scatter plots of QBO westerly phase minus easterly phase for ~~50~~ 30 hPa zonal wind anomalies and 70 hPa ~~water vapor~~WV anomalies with a lag of 6 months averaged between 5°S-5°N among models for the northern summer and (b) the northern winter. ~~(c-f) Composite of the 7 CMIP6 models in summer and 5 CMIP6 models in winter under different QBO phases.~~

6 Summary and discussions

Based on ERA5 reanalysis and SWOOSH observations, this study investigates the ~~water vapor~~WV QBO phenomenon in the stratosphere. The distribution of the ~~stratospheric water vapor~~SWV under different QBO phases in northern winter and summer is compared. The possible causes for the ~~water vapor~~WV variability associated with the QBO are discussed, including the stratospheric circulation, temperature, and residual circulation variations. Simulations of the ~~stratospheric water vapor~~SWV QBO are also evaluated for 18 CMIP6 high-top models using the historical run data.

I. Previous studies have used SWOOSH and some climate models to analyze the tropical S~~stratospheric water vapor~~WV entry associated with QBO (e.g., Ziskin et al., 2022). Here we focus on the QBO signals using a 15-60-month bandpass filtering of ~~stratospheric water vapor~~SWV in the deep tropics (averaged over 5°N-5°S latitude band), the tropical ~~stratospheric water vapor~~SWV presents obvious QBO variability, and the maximum ~~water vapor~~WV QBO signals propagate regularly from the lowermost to middle and lower stratosphere around 10-100 hPa. The 30 hPa QBO index exerts the greatest influence on 100 hPa WV at a lag of six months, and previous studies have also discussed the lag effect of the QBO index on WV in the low stratosphere (Diallo et al., 2022; Ziskin et al., 2022). Anomalous moistening typically occurs during the QBO westerly phase, while anomalous drying occurs during the QBO easterly phase. During northern summer, the peak amplitude of 100 hPa WV under different QBO phases in tropical regions reaches ±0.12 ppm

at a six-month lag, while in winter it reaches ±0.2 ppm. The difference of WV distribution in the lower stratosphere between westerly and easterly QBO phases in summer is smaller than in winter, which has not been reported in the relevant literature.~~The water vapuring the QBO westerly phase, while anomalous drying during the QBO easterly phase. Separate analysis on the water vapor QBO in the northern winter and summer reveals that the difference of water vapor distribution in the lower stratosphere between westerly and easterly QBO phases in summer is much smaller than in winter. Further, the water vapor QBO is also observed in the upper stratosphere around 2–5 hPa, although the water vapor anomalies are less significantly correlated with the zonal wind anomalies.~~

II. The ~~Difference in the secondary circulation associated with QBO between winter and summer is compared. In the northern summer, due to the dynamic effect of the QBO, two anomalous secondary circulation cells form in the lower and middle stratosphere over the tropics and the Southern Hemisphere subtropics region, respectively. The two secondary cells in the QBO westerly phase are opposite to those in the QBO easterly phase. The net effect is that the temperature anomalies manifest as a quadrupole distribution spanning the tropics and subtropics, with warm anomalies collocated with anomalous downwelling and cold anomalies collocated with anomalous upwelling. In the northern winter, the subtropical cell in the lower and middle stratosphere shifts to the Northern Hemisphere subtropics. These two secondary circulation cells are opposite under the easterly and westerly phases of QBO. The intensity of BD circulation anomalies in winter is obviously stronger than that in summer. Diagnosis of the transformed Eulerian Mean (TEM) tracer continuity equation reveals that the mean advection term by the residual circulation associated with the QBO is the leading factor controlling the water vapor distribution in most of the stratosphere.~~tropopause cold point temperature in the tropics affects the tropospheric ~~water vapor~~WV entering the stratosphere (Garfinkel et al., 2013; Randel and Park, 2019). Consistent with previous work (Tegtmeier et al., 2020), the 100 hPa temperature in the tropics shows warm anomalies under the QBO westerly phase and cold anomalies under the easterly QBO phase. However, the intensity and coverage of tropical temperature anomalies in winter are significantly greater and broader than that in summer, which is consistent with the BD circulation anomalies being significantly stronger in winter than in summer. As the QBO signal propagates downward from the upper stratosphere, the 30 hPa QBO index has a significant impact on the 100 hPa temperature after six months, but the lagged temperature amplitude in northern summer is still smaller than that in winter.~~Additionally, OLR anomalies show opposite changes under both QBO phases in the northern winter and summer, respectively. The influence of OLR on the tropopause cold point temperature in summer is reversed with the tropical stratospheric low temperature anomalies, which further reduces the temperature anomaly magnitude around 100 hPa in summer. In northern winter, the effect of OLR on the cold point temperature is superimposed with the tropical lower stratospheric temperature anomaly, which amplifies the temperature difference between the easterly and westerly QBO phases.~~

III. ~~The~~ The difference in the secondary circulation associated with QBO between winter and summer is compared. The secondary circulation related to QBO is opposite in the easterly and westerly phases (Baldwin et al., 2001)~~In the northern summer, due to the dynamic effect of the QBO, two anomalous secondary circulation cells form in the lower and middle stratosphere over the tropics and the Southern Hemisphere subtropics region, respectively. The two secondary cells in the~~

~~QBO westerly phase are opposite to those in the QBO easterly phase. The net effect is that the temperature anomalies manifest as a quadrupole distribution spanning the tropics and subtropics, with warm anomalies collocated with anomalous downwelling and cold anomalies collocated with anomalous upwelling. In the northern winter, the subtropical cell in the lower and middle stratosphere shifts to the Northern Hemisphere subtropics~~. The intensity of the QBO-related residual secondary circulation is stronger in the boreal winter than in summer, which not only influences the cold point tropopause temperature in tropical regions but also drives the transport of SWV.~~These two secondary circulation cells are opposite under the easterly and westerly phases of QBO. The intensity of BD circulation anomalies in winter is obviously stronger than that in summer.~~ Diagnosis of the transformed Eulerian-Mean (TEM) tracer continuity equation reveals that the mean advection term by the residual circulation associated with the QBO is the leading factor controlling the ~~water vapor~~ WV distribution in the tropical lower stratosphere~~in most of the stratosphere~~. ~~tropopause cold point temperature in the tropics affects the tropospheric water vapor entering the stratosphere (Garfinkel et al., 2013; Randel and Park, 2019). Consistent with previous work, the 100 hPa temperature in the tropics shows warm anomalies under the QBO westerly phase and cold anomalies under the easterly QBO phase. However, the intensity and coverage of tropical temperature anomalies in winter are significantly greater and broader than that in summer, which is consistent with the BD circulation anomalies being significantly stronger in winter than in summer. Additionally, OLR anomalies show opposite changes under both QBO phases in the northern winter and summer, respectively. The influence of OLR on the tropopause cold point temperature in summer is reversed with the tropical stratospheric low temperature anomalies, which further reduces the temperature anomaly magnitude around 100 hPa in summer. In northern winter, the effect of OLR on the cold point temperature is superimposed with the tropical lower stratospheric temperature anomaly, which amplifies the temperature difference between the easterly and westerly QBO phases.~~

IV. Among the 18 CMIP6 high-top models that can produce the QBO spontaneously, 11 models can simulate upward propagation of the ~~water vapor~~WV QBO from the lowermost to middle stratosphere around 10–100 hPa, though for all models the signal is too weak. The CMIP6 model can simulate the lag effect of the 30 hPa QBO index on WV in the low stratosphere. The QBO index amplitude in some models is close to that of ERA5, but the amplitude of WV is very small.~~Eight models simulate water vapor QBO in the upper stratosphere between 1–5 hPa, although divergence exists for the depth of the water vapor QBO among CMIP6 models.~~ A model-by-model examination also reveals that the seasonal difference in the ~~water vapor~~WV QBO can be reproduced by very few models, which ~~challenge~~ challenges the model developers to well tune the simulation of the QBO itself and its climate effect.

The change of ~~stratospheric S~~water vapor WV can be traced back to the change of the cold point temperature at the bottom of the tropical stratosphere (Hardiman et al., 2015; Xia et al., 2019). The cold point temperature variability is a comprehensive effect from the stratospheric (from top to bottom) and tropospheric (from bottom to top) dynamics. In this study, the influence of stratospheric QBO on ~~water vapor~~WV is considered, and the bottom-up influence from ENSO and sea surface temperature in the Indo-Pacific oceans is not considered. However, this study reveals the difference in S~~tratospheric water vapor~~WV content regulated by QBO between northern winter and summer, and finds that QBO-related cold point temperature anomalies

in the tropics affect ~~water vapor~~WV distribution in the lower tropical stratosphere with a 6-month lag. QBO-related secondary circulation affects ~~water vapor~~WV transport in the middle and ~~upper~~lower tropical stratosphere, which ~~However, this study reveals the difference of the stratospheric water vapor QBO between winter and summer, and finds that BD circulation change related to QBO might be a mediator bridging the QBO and water vapor. It~~ provides a new perspective to better understand the ~~stratospheric water vapor~~SWV QBO signals. As the dominant mode of the tropical stratosphere, a detailed analysis of the QBO modulation on ~~water vapor~~WV ~~QBO~~ signals is also a prerequisite to improve the performance of climate models for a better simulation of stratospheric variability and its role in subseasonal to seasonal forecasts.

Acknowledgments

The work was supported by the National Natural Science Foundation of China (42361144843, 42322503, and 42175069), Israel Science Foundation (3065/23). NSFC and ISF are acknowledged for their funding. The authors thank ECMWF (https://cds.climate.copernicus.eu) for their providing the ERA5 reanalysis data. The SWOOSH data set version 2.7 is obtained from https://csl.noaa.gov/groups/csl8/swoosh/. The CMIP6 data are provided by the WCRP (https://aims2.llnl.gov/search/cmip6).

Autor contribution

QL and JR designed the study. QL analyzed the data and wrote the manuscript. CS and CIG contributed to the discussion and revision of the paper.

References

Abalos, M., Calvo, N., Benito-Barca, S., Garny, H., Hardiman, S. C., Lin, P., Andrews, M. B., Butchart, N., Garcia, R., Orbe, C., Saint-Martin, D., Watanabe, S., and Yoshida, K.: The Brewer-Dobson circulation in CMIP6, Atmos. Chem. Phys., 21, 13571–13591, https://doi.org/10.5194/acp-21-13571-2021, 2021.

Allen, R. J. and Sherwood, S. C.: Warming maximum in the tropical upper troposphere deduced from thermal winds, Nat. Geosci., 1, 399–403, https://doi.org/10.1038/ngeo208, 2008.

Anstey, J. A., Osprey, S. M., Alexander, J., Baldwin, M. P., Butchart, N., Gray, L., Kawatani, Y., Newman, P. A., and Richter, J. H.: Impacts, processes and projections of the quasi-biennial oscillation, Nat. Rev. Earth Environ., 3, 588–603, https://doi.org/10.1038/s43017-022-00323-7, 2022.

Baldwin, M. P., Gray, L. J., Dunkerton, T. J., Hamilton, K., Haynes, P. H., Holton, J. R., Alexander, M. J., Hirota, I., Horinouchi, T., Jones, D. B. A., Marquardt, C., Sato, K., and Takahashi, M.: The quasi-biennial oscillation, Rev. Geophys., 39, 179–229, 2001.

Banerjee, A., Chiodo, G., Previdi, M., Ponater, M., Conley, A. J., and Polvani, L. M.: Stratospheric water vapor: an important climate feedback, Clim. Dyn., 53, 1697–1710, https://doi.org/10.1007/s00382-019-04721-4, 2019.

Bi, Y., Chen, Y., Zhou, R., Yi, M., and Deng, S.: Simulation of the effect of water-vapor increase on temperature in the stratosphere, Adv. Atmos. Sci., 28, 832–842, https://doi.org/10.1007/s00376-010-0047-7.1, 2011.

Bramberger, M., Alexander, M. J., Davis, S., Podglajen, A., Hertzog, A., Kalnajs, L., Deshler, T., Goetz, J. D., and Khaykin, S.: First super-pressure Balloon-Borne fine-vertical-scale profiles in the upper TTL: impacts of atmospheric waves on cirrus clouds and the QBO, Geophys. Res. Lett., 49, e2021GL097596, https://doi.org/10.1029/2021GL097596, 2022.

Brewer, A. W.: Evidence for a world circulation provided by the measurements of helium and water vapor distribution in the stratosphere, Q. J. R. Meteorol. Soc., 75, 351–363, https://doi.org/10.1002/qj.49707532603, 1949.

Butchart, N.: The Brewer-Dobson circulation, Rev. Geophys., 52, 157–184, https://doi.org/10.1002/2013RG000448.One, 2014.

Butchart, N., Anstey, J. A., Hamilton, K., Osprey, S., McLandress, C., Bushell, A. C., Kawatani, Y., Kim, Y.-H., Lott, F., Scinocca, J., Stockdale, T. N., Andrews, M., Bellprat, O., Braesicke, P., Cagnazzo, C., Chen, C.-C., Chun, H.-Y., Dobrynin, M., Garcia, R. R., Garcia-Serrano, J., Gray, L. J., Holt, L., Kerzenmacher, T., Naoe, H., Pohlmann, H., Richter, J. H., Scaife, A. A., Schenzinger, V., Serva, F., Versick, S., Watanabe, S., Yoshida, K., Yukimoto, S.: Overview of experiment design and comparison of models participating in phase 1 of the SPARC quasi-biennial oscillation initiative (QBOi), Geosci. Model Dev., 11, 1009–1032, https://doi.org/10.5194/gmd-11-1009-2018, 2018.

Cai, Q., Chen, W., Chen, S., Ma, T., and Garfinkel, C. I.: Influence of the quasi-biennial oscillation on the spatial structure of the wintertime Arctic oscillation, J. Geophys. Res. Atmos., 127, https://doi.org/10.1029/2021JD035564, 2022.

Canziani, P. O. and Holton, J. R.: Kelvin Waves and the quasi-biennial oscillation: An observational analysis, J. Geophys. Res. Atmos., 103, 31509–31521, https://doi.org/10.1029/1998JD200021, 1998.

Charlesworth, E., Plöger, F., Birner, T., Baikhadzhaev, R., Abalos, M., Abraham, N. L., Akiyoshi, H., Bekki, S., Dennison, F., Jöckel, P., Keeble, J., Kinnison, D., Morgenstern, O., Plummer, D., Rozanov, E., Strode, S., Zeng, G., Egorova, T., and Riese, M.: Stratospheric water vapor affecting atmospheric circulation, Nat. Commun., 14, 3925, https://doi.org/10.1038/s41467-023-39559-2, 2023.

Chen, Y., Shi, C., and Zheng, B.: HCl quasi-biennial oscillation in the stratosphere and a comparison with ozone QBO, Adv. Atmos. Sci., 22, 751–758, https://doi.org/10.1007/BF02918718, 2005.

Coy, L., Newman, P. A., Pawson, S., and Lait, L. R.: Dynamics of the disrupted 2015/16 quasi-biennial oscillation, J. Clim., 30, 5661–5674, https://doi.org/10.1175/JCLI-D-16-0663.1, 2017.

Davis, S. M., Rosenlof, K. H., Hassler, B., Hurst, D. F., Read, W. G., Vömel, H., Selkirk, H., Fujiwara, M., and Damadeo, R.: The stratospheric water and ozone satellite homogenized (SWOOSH) database: A long-term database for climate studies, Earth Syst. Sci. Data, 8, 461–490, https://doi.org/10.5194/essd-8-461-2016, 2016.

Dessler, A. E., Schoeberl, M. R., Wang, T., Davis, S. M., and Rosenlof, K. H.: Stratospheric water vapor feedback, Proc. Natl. Acad. Sci. U. S. A., 110, 18087–18091, https://doi.org/10.1073/pnas.1310344110, 2013.

Diallo, M. A., Ploeger, F., Hegglin, M. I., Ern, M., Grooß, J.-U., Khaykin, S., and Riese, M.: Stratospheric water vapour and ozone response to the quasi-biennial oscillation disruptions in 2016 and 2020, Atmos. Chem. Phys., 22, 14303–14321, https://doi.org/10.5194/acp-22-14303-2022, 2022.

Dong, W. H., Lin, Y. L., Zhang, M. H., and Huang, X. M.: Footprint of tropical mesoscale convective system variability on stratospheric water vapor, Geophys. Res. Lett., 47, e2019GL086320, https://doi.org/10.1029/2019GL086320, 2020.

Evan, S., Rosenlof, K. H., Thornberry, T., and Khaykin, S.: TTL cooling and drying during the January 2013 stratospheric sudden warming, Q. J. R. Meteorol. Soc., 3030–3039, https://doi.org/10.1002/qj.2587, 2015.

Eyring, V., Bony, S., Meehl, G. A., Senior, C. A., Stevens, B., Stouffer, R. J., Taylor, K. E., Dynamique, D. M., Pierre, I., Laplace, S., and Ipsl, L. M. D.: Overview of the coupled model intercomparison project phase 6 (CMIP6) experimental design and organization, Geosci. Model Dev., 9, 1937–1958, https://doi.org/10.5194/gmd-9-1937-2016, 2016.

de Forster, P. M. and Shine, K. P.: Stratospheric water vapor changes as a possible contributor to observed stratospheric cooling, Geophys. Res. Lett., 26, 3309–3312, https://doi.org/10.1029/1999GL010487, 1999.

Fueglistaler, S., Dessler, A. E., Dunkerton, T. J., Folkins, I., Fu, Q., and Mote, P. W.: Troplical tropopause layer, Rev. Geophys., 47, RG1004, https://doi.org/10.1029/2008RG000267.1, 2009.

Garcia, R. R. and Solomon, S.: A numerical model of the zonally averaged dynamical and chemical structure of the middle atmosphere, J. Geophys. Res. Ocean., 88, 1379–1400, https://doi.org/https://doi.org/10.1029/JC088iC02p01379, 1983.

Garfinkel, C. I., Waugh, D. W., Oman, L. D., Wang, L., and Hurwitz, M. M.: Temperature trends in the tropical upper troposphere and lower stratosphere-: Connections with sea surface temperatures and implications for water vapor and ozone, J. Geophys. Res. Atmos., 118, 9658–9672, https://doi.org/10.1002/jgrd.50772, 2013.

Garfinkel, C. I., Harari, O., Ziskin Ziv, S., Rao, J., Morgenstern, O., Zeng, G., Tilmes, S., Kinnison, D., O'Connor, F. M., Butchart, N., Deushi, M., Jöckel, P., Pozzer, A., and Davis, S.: Influence of the El Nino-Southern Oscillation on entry stratospheric water vapor in coupled chemistry-ocean CCMI and CMIP6 models, Atmos. Chem. Phys., 21, 3725–3740, https://doi.org/10.5194/acp-21-3725-2021, 2021.

Garfinkel, C. I., Gerber, E. P., Shamir, O., Rao, J., Jucker, M., White, I., and Paldor, N.: A QBO cookbook: Sensitivity of the Quasi-Biennial Oscillation to resolution, resolved waves, and parameterized gravity waves, J. Adv. Model. Earth Syst., 14, 1–17, https://doi.org/10.1029/2021MS002568, 2022.

Geller, M. A., Zhou, T., Shindell, D., Ruedy, R., Aleinov, I., Nazarenko, L., Tausnev, N. L., Kelley, M., Sun, S., Cheng, Y., Field, R. D., Faluvegi, G.: Modeling the QBO—Improvements resulting from higher-model vertical resolution, J. Adv. Model. Earth Syst., 8, 1092–1105, https://doi.org/10.1002/2016MS000699, 2016.

Gettelman, A. and Birner, T.: Insights into tropical tropopause layer processes using global models, J. Geophys. Res. Atmos., 112, 1–15, https://doi.org/10.1029/2007JD008945, 2007.

Hardiman, S. C., Butchart, N., and Calvo, N.: The morphology of the Brewer-Dobson circulation and its response to climate change in CMIP5 simulations, Q. J. R. Meteorol. Soc., 140, 1958–1965, https://doi.org/10.1002/qj.2258, 2014.

Hardiman, S. C., Boutle, I. A., Bushell, A. C., Butchart, N., Cullen, M. J. P., Field, P. R., Furtado, K., Manners, J. C., Milton, S. F., Morcrette, C., O'Connor, F. M., Shipway, B. J., Smith, C., Walters, D. N., Willett, M. R., Williams, K. D., Wood, N., Abraham, N. L., Keeble, J., Maycock, A. C., Thuburn, J., and Woodhouse, M. T.: Processes controlling tropical tropopause temperature and stratospheric water vapor in climate models, J. Clim., 28, 6516–6535, https://doi.org/https://doi.org/10.1175/JCLI-D-15-0075.1, 2015.

Held, I. M. and Soden, B. J.: Water vapor feedback and global warming, Annu. Rev. Energy Environ., 25, 441–475, https://doi.org/10.1146/annurev.energy.25.1.441, 2000.

Hersbach, H., Bell, B., Berrisford, P., Hirahara, S., Horányi, A., Muñoz-Sabater, J., Nicolas, J., Peubey, C., Radu, R., Schepers, D., Simmons, A., Soci, C., Abdalla, S., Abellan, X., Balsamo, G., Bechtold, P., Biavati, G., Bidlot, J., Bonavita, M., De Chiara, G., Dahlgren, P., Dee, D., Diamantakis, M., Dragani, R., Flemming, J., Forbes, R., Fuentes, M., Geer, A., Haimberger, L., Healy, S., Hogan, R. J., Hólm, E., Janisková, M., Keeley, S., Laloyaux, P., Lopez, P., Lupu, C., Radnoti, G., de Rosnay, P., Rozum, I., Vamborg, F., Villaume, S., and Thépaut, J. N.: The ERA5 global reanalysis, Q. J. R. Meteorol. Soc., 146, 1999–2049, https://doi.org/10.1002/qj.3803, 2020.

Holt, L. A., Alexander, M. J., Coy, L., Molod, A., Putman, W., and Pawson, S.: Tropical waves and the quasi-biennial oscillation in a 7-km global climate simulation, J. Atmos. Sci., 73, 3771–3783, https://doi.org/10.1175/JAS-D-15-0350.1, 2016.

Holton, J. R. and Gettelman, A.: Horizontal transport and the dehydration of the stratosphere, Geophys. Res. Lett., 28, 2799–2802, https://doi.org/10.1029/2001GL013148, 2001.

Holton, J. R., Haynes, P. H., Mcintyre, M. E., Douglass, A. R., and Rood, B.: Stratonsphere-Troposphere exchange, Rev. Geophys., 33, 403–439, https://doi.org/10.1029/95RG02097, 1995.

Kang, M. J., Chun, H. Y., and Garcia, R. R.: Role of equatorial waves and convective gravity waves in the 2015/16 quasi-biennial oscillation disruption, Atmos. Chem. Phys., 20, 14669–14693, https://doi.org/10.5194/acp-20-14669-2020, 2020.

Keeble, J., Hassler, B., Banerjee, A., Checa-Garcia, R., Chiodo, G., Davis, S., Eyring, V., Griffiths, P. T., Morgenstern, O., Nowack, P., Zeng, G., Zhang, J., Bodeker, G., Burrows, S., Cameron-Smith, P., Cugnet, D., Danek, C., Deushi, M., Horowitz, L. W., Kubin, A., Li, L., Lohmann, G., Michou, M., Mills, M. J., Nabat, P., Olivié, D., Park, S., Seland, Ø., Stoll, J., Wieners, K. H., and Wu, T.: Evaluating stratospheric ozone and water vapor changes in CMIP6 models from 1850 to 2100, Atmos. Chem. Phys., 21, 5015–5061, https://doi.org/10.5194/acp-21-5015-2021, 2021.

Kim, J., Randel, W. J., and Birner, T.: Convectively driven tropopause-level cooling and its influences on stratospheric moisture, J. Geophys. Res. Atmos., 123, 590–606, https://doi.org/10.1002/2017JD027080, 2018.

Krishnamurti, T. N., Subramaniam, M., Oosterhof, D. K., and Daughenbaugh, G.: Predictability of low frequency modes, Meteorol. Atmos. Phys., 44, 63–83, https://doi.org/10.1007/BF01026811, 1990.

Krüger, K., Schäfler, A., Wirth, M., Weissmann, M., Craig, G. C.: Vertical structure of the lower-stratospheric moist bias in the ERA5 reanalysis and its connection to mixing processes, Atmos. Chem. Phys., 22, 15559-15577, https://doi.org/10.5194/acp-22-15559-2022, 2022.

Lindzen, R. S. and Holton, J. R.: A Theory of the Quasi-Biennial Oscillation, J. Atmos. Sci., 25, 1095–1107, https://doi.org/https://doi.org/10.1175/1520-0469(1968)025<1095:ATOTQB>2.0.CO;2, 1968.

Lu, J., Xie, F., Sun, C., Luo, J., Cai, Q., Zhang, J., Li, J., and Tian, H.: Analysis of factors influencing tropical lower stratospheric water vapor during 1980–2017, npj Clim. Atmos. Sci., 3, 35, https://doi.org/10.1038/s41612-020-00138-7, 2020.

Lott, F., Denvil, S., Butchart, N., Cagnazzo, C., Giorgetta, M. A., Hardiman, S. C., Manzini, E., Krismer, T., Duvel J.-P., Maury, P., Scinocca, J. F., Watanabe, S., Yukimoto, S.: Kelvin and Rossby-gravity wave packets in the lower stratosphere of some high-top CMIP5 models, J. Geophys. Res. Atmos., 119, 2156–2173, https://doi.org/10.1002/2013JD020797, 2014.

Monier, E. and Weare, B. C.: Climatology and trends in the forcing of the stratospheric ozone transport, Atmos. Chem. Phys., 11, 6311–6323, https://doi.org/10.5194/acp-11-6311-2011, 2011.

Mote, P. W., Rosenlof, K. H., Mclntyre, M. E., Carr, E. S., Gille, J. C., Holton, J. R., Kinnersley, S., Pumphrey, H. C., Iii, J. M. R., and Vaters, J. W.: An atmospheric tape recorder: The imprint of tropical tropopause temperatures on stratospheric water vapor, J. Geophys. Res., 101, 3989–4006, https://doi.org/10.1029/95JD03422, 1996.

Mote, P. W., Clark, H. L., Dunkerton, T. J., Harwood, R. S., and Pumphrey, H. C.: Intraseasonal variations of water vapor in the tropical upper troposphere and tropopause region, J. Geophys. Res. Atmos., 105, 17457–17470, https://doi.org/10.1029/2000JD900158, 2000.

Muhsin, M., Sunilkumar, S. V, Venkat Ratnam, M., Parameswaran, K., Krishna Murthy, B. V, and Emmanuel, M.: Effect of convection on the thermal structure of the troposphere and lower stratosphere including the tropical tropopause layer in the South Asian monsoon region, J. Atmos. Solar-Terrestrial Phys., 169, 52–65, https://doi.org/https://doi.org/10.1016/j.jastp.2018.01.016, 2018.

Murakami, M.: Large-scale aspects of deep convective activity over the GATE, Mon. Weather Rev., 107, 994–1013, https://doi.org/https://doi.org/10.1175/1520-0493(1979)107<0994:LSAODC>2.0.CO;2, 1979.

Pahlavan, H. A., Wallace, J. M., and Fu, Q.: Characteristics of tropical convective gravity waves resolved by ERA5 reanalysis, J. Atmos. Sci., 80, 777–795, https://doi.org/10.1175/JAS-D-22-0057.1, 2023.

Peña-Ortiz, C., Plaza, N. P., Gallego, D., and Ploeger, F.: Quasi-biennial oscillation modulation of stratospheric water vapour in the Asian monsoon, Atmos. Chem. Phys., 24, 5457–5478, https://doi.org/10.5194/acp-24-5457-2024, 2024.

Randel, W. and Park, M.: Diagnosing observed stratospheric water vapor relationships to the cold point tropical tropopause, J. Geophys. Res. Atmos., 124, 7018–7033, https://doi.org/10.1029/2019JD030648, 2019.

Randel, W. J. and Wu, F.: Kelvin wave variability near the equatorial tropopause observed in GPS radio occultation measurements, J. Geophys. Res., 110, 1–13, https://doi.org/10.1029/2004JD005006, 2005.

Randel, W. J., Zhang, K., and Fu, R.: What controls stratospheric water vapor in the NH summer monsoon regions?, J. Geophys. Res. Atmos., 120, 7988–8001, https://doi.org/10.1002/2015JD023622, 2015.

Rao, J., Yu, Y., Guo, D., Shi, C., Chen, D., and Hu, D.: Evaluating the Brewer–Dobson circulation and its responses to ENSO, QBO, and the solar cycle in different reanalyses, Earth Planet. Phys., 3, 166–181, https://doi.org/https://doi.org/10.26464/epp2019012, 2019.

Rao, J., Garfinkel, C. I., and White, I. P.: How does the quasi-biennial oscillation affect the boreal winter tropospheric circulation in cmip5/6 models?, J. Clim., 33, 8975–8996, https://doi.org/10.1175/JCLI-D-20-0024.1, 2020a.

Rao, J., Garfinkel, C. I., and White, I. P.: Impact of the quasi-biennial oscillation on the northern winter stratospheric polar vortex in CMIP5/6 models, J. Clim., 33, 4787–4813, https://doi.org/10.1175/JCLI-D-19-0663.1, 2020b.

Rao, J., Garfinkel, C. I., Ren, R., Wu, T., Lu, Y., and Chu, M.: Projected strengthening impact of the quasi-biennial oscillation on the Southern Hemisphere by CMIP5/6 Models, J. Clim., 36, 5461–5476, https://doi.org/10.1175/JCLI-D-22-0801.1, 2023a.

Rao, J., Garfinkel, C. I., Ren, R., Wu, T., and Lu, Y.: Southern Hemisphere response to the quasi-biennial oscillation in the CMIP5/6 models, J. Clim., 36, 2603–2623, https://doi.org/10.1175/JCLI-D-22-0675.1, 2023b.

Ricciardulli, L., Garcia, R. R.: The Excitation of Equatorial Waves by Deep Convection in the NCAR Community Climate Model (CCM3), J. Atmos. Sci., 57, 3461–3487, https://doi.org/10.1175/1520-0469(2000)057<3461:TEOEWB>2.0.CO;2, 2000.

Richter, J. H., Solomon, A., and Bacmeister, J. T.: Effects of vertical resolution and nonpornographic gravity wave drag on the simulated climate in the Community Atmosphere Model, version 5, J. Adv. Model. Earth Syst., 6, 92–95, https://doi.org/10.1002/2013MS000303~~.Received~~, 2014a.

Richter, J. H., Solomon, A., and Bacmeister, J. T.: On the simulation of the quasi-biennial oscillation in the Community Atmosphere Model, version 5, J. Geophys. Res. Atmos., 119, 3045–3062, https://doi.org/10.1002/2013JD021122, 2014b.

Richter, J. H., Anstey, J. A., Butchart, N., Kawatani, Y., Meehl, G. A., Osprey, S., Simpson, I. R.: Progress in simulating the quasi-biennial oscillation in CMIP models, J. Geophys. Res. Atmos., 125, e2019JD032362, https://doi.org/10.1029/2019JD032362, 2020.

Serva, F., Anstey, J. A., Bushell, A. C., Butchart, N., Cagnazzo, C., Gray, L. J., Kawatani, Y., Osprey, S. M., Richter, J. H., and Simpson, I. R.: The impact of the QBO on the region of the tropical tropopause in QBOi models: Present-day simulations, Q. J. R. Meteorol. Soc., 148, 1945–1964, https://doi.org/10.1002/qj.4287, 2022.

Simmons, A., Soci, C., Nicolas J.: Global stratospheric temperature bias and other stratospheric aspects of ERA5 and ERA5.1, Series: ECMWF Technical Memoranda, 859, 1-38, https://doi.org/10.21957/rcxqfmg0, 2020.

Simpkins, G.: Progress in climate modeling, Nat. Clim. Chang., 7, 684–685, https://doi.org/10.1038/nclimate3398, 2017.

Solomon, S., Rosenlof, K. H., Portmann, R. W., Daniel, J. S., Davis, S. M., Sanford, T. J., and Plattner, G. K.: Contributions of stratospheric water vapor to decadal changes in the rate of global warming, Science 80, 327, 1219–1223, https://doi.org/10.1126/science.1182488, 2010.

Tao, M., Konopka, P., Ploeger, F., Riese, M., Müller, R., and Volk, C. M.: Impact of stratospheric major warmings and the quasi-biennial oscillation on the variability of stratospheric water vapor, Geophys. Res. Lett., 42, 4599–4607, https://doi.org/10.1002/2015GL064443, 2015.

Tegtmeier, S., Anstey, J., Davis, S., Ivanciu, I., Jia, Y., McPhee, D., and Pilch Kedzierski, R.: Zonal asymmetry of the qbo temperature signal in the tropical tropopause region, Geophys. Res. Lett., 47, 1–10, https://doi.org/10.1029/2020GL089533, 2020.

Tian, W., Chipperfield, M. P., and Lv, D.: Impact of increasing stratospheric water vapor on ozone depletion and temperature change, Adv. Atmos. Sci., 26, 423–437, https://doi.org/10.1007/s00376-009-0423-3.1, 2009.

Tian, W., Huang, J., and Zhang, J.: Role of stratospheric processes in climate change: Advances and Challenges, Adv. Atmos. Sci.,, 40, 1379−1400, https://doi.org/10.1007/s00376-023-2341-1, 2023.

Tinney, E. N. and Homeyer, C. R.: Climatology, sources, and transport characteristics of observed water vapor extrema in the lower stratosphere, Atmos. Chem. Phys., 23, 14375–14392, https://doi.org/10.5194/acp-23-14375-2023, 2023.

Tselioudis, G., Tromeur, E., Rossow, W. B., and Zerefos, C. S.: Decadal changes in tropical convection suggest effects on stratospheric water vapor, Geophys. Res. Lett., 37, L14806, https://doi.org/10.1029/2010GL044092, 2010.

Ueyama, R., Schoeberl, M., Jensen, E., Pfister, L., Park, M., and Ryoo, J.: Convective impact on the global lower stratospheric water vapor budget, J. Geophys. Res. Atmos., 128, e2022JD037135, https://doi.org/10.1029/2022JD037135, 2016.

Wallace, J. M. and Kousky, V. E.: Observational evidence of kelvin waves in the tropical stratosphere, J. Atmos. Sci., 25, 900–907, https://doi.org/https://doi.org/10.1175/1520-0469(1968)025<0900:OEOKWI>2.0.CO;2, 1968.

Wang, T., Zhang, Q., Hannachi, A., Hirooka, T., Hegglin, MI.: Tropical water vapor in the lower stratosphere and its relationship to tropical/extratropical dynamical processes in ERA5, Q. J. R. Meteorol. Soc., 146, 2432–2449, https://doi.org/10.1002/qj.3801, 2020.

Wang, Y., Rao, J., Lu, Y., Ju, Z., Yang, J., and Luo, J.: A revisit and comparison of the quasi-biennial oscillation (QBO) disruption events in 2015/16 and 2019/20, Atmos. Res., 294, 106970, https://doi.org/https://doi.org/10.1016/j.atmosres.2023.106970, 2023.

Wohltmann, I., Santee, M. L., Manney, G. L., and Luis F. Millán: The chemical effect of increased water vapor from the Hunga Tongaeruption on the Antarctic, Geophys. Res. Lett., 51, e2023GL106980, https://doi.org/10.1029/2023GL106980, 2024.

Xia, Y., Huang, Y., Hu, Y., and Yang, J.: Impacts of tropical tropopause warming on the stratospheric water vapor, Clim. Dyn., 53, 3409–3418, https://doi.org/10.1007/s00382-019-04714-3, 2019.

Xia, Y., Huang, Y., Hu, Y., and Yang, J.: Lower stratospheric water vapor variations diagnosed from satellite observations, reanalysis data, and a chemistry-climate model, J. Meteorol. Res., 35, 701–715, https://doi.org/10.1007/s13351-021-0193-0, 2021.

Ye, H., Dessler, A. E., and Yu, W.: Effects of convective ice evaporation on interannual variability of tropical tropopause layer water vapor, Atmos. Chem. Phys., 18, 4425–4437, https://doi.org/10.5194/acp-18-4425-2018, 2018.

Yue, J., Russell, J., Gan, Q., Wang, T., Rong, P., Garcia, R., and Mlynczak, M.: Increasing water vapor in the stratosphere and mesosphere after 2002, Geophys. Res. Lett., 46, 13452–13460, https://doi.org/10.1029/2019GL084973, 2019.

Ziskin Ziv, S., Garfinkel, C. I., Davis, S., and Banerjee, A.: The roles of the Quasi-Biennial Oscillation and El Niño for entry stratospheric water vapor in observations and coupled chemistry-ocean CCMI and CMIP6 models, Atmos. Chem. Phys., 22, 7523–7538, https://doi.org/10.5194/acp-22-7523-2022, 2022.